

Target Localization and Tracking in Noncoherent Multiple-Input Multiple-Output Radar Systems

RUIXIN NIU, Senior Member, IEEE

RICK S. BLUM, Fellow, IEEE

PRAMOD K. VARSHNEY, Fellow, IEEE

ANDREW L. DROZD, Fellow, IEEE

For a noncoherent multiple-input multiple-output (MIMO) radar system, the maximum likelihood estimator (MLE) of the target location and velocity, as well as the corresponding Cramér-Rao lower bound (CRLB) matrix, is derived. MIMO radar's potential in localization and tracking performance is demonstrated by adopting simple Gaussian pulse waveforms. Due to the short duration of the Gaussian pulses, a very high localization performance can be achieved, even when the matched filter ignores the Doppler effect by matching to zero Doppler shift. This leads to significantly reduced complexities for the matched filter and the MLE. Further, two interactive signal processing and tracking algorithms, based on the Kalman filter and the particle filter (PF), respectively, are proposed for noncoherent MIMO radar target tracking. For a system with a large number of transmit/receive elements and a high signal-to-noise ratio (SNR) value, the Kalman filter (KF) is a good choice; while for a system with a small number of elements and a low SNR value, the PF outperforms the KF significantly. In both methods, the tracker provides predictive information regarding the target location, so that the matched filter can match to the most probable target locations, reducing the complexity of the matched filter and improving the tracking performance. Since tracking is performed without detection, the presented approach can be deemed as a track-before-detect approach. It is demonstrated through simulations that the noncoherent MIMO radar provides significant tracking performance improvement over a monostatic phased array radar with high range and azimuth resolutions. Further, the effects of coherent integration of pulses are investigated for both the phased array radar and a hybrid MIMO radar, where only the pulses transmitted and received by colocated transceivers are coherently integrated and the other pulses are combined noncoherently. It is shown that the hybrid MIMO radar achieves significant tracking performance improvement when compared with the phased array radar, by using the extra Doppler information obtained through coherent pulse integration.

Manuscript received June 19, 2010; revised February 1, 2011; released for publication May 17, 2011.

IEEE Log No. T-AES/48/2/943829.

Refereeing of this contribution was handled by S. Blunt.

This work was supported in part by U.S. Army Space and Missile Defense Command and the Missile Defense Agency under Contracts HQ0006-06-C-7504 Phase I and W9113M-08-C-0221.

This work was presented in part at Asilomar'09, Pacific Grove, CA, November 2009.

Authors' addresses: R. Niu, Department of Electrical and Computer Engineering, Virginia Commonwealth University, 601 West Main Street, Richmond, VA 23284, E-mail: (rniu@vcu.edu);

P. K. Varshney, Department of Electrical and Computer Science, Syracuse University, 4-206 Center for Science and Technology, Syracuse, NY 13244; R. S. Blum, Department of Electrical and Computer Engineering, Lehigh University, 304 Packard Lab, 19 Memorial Drive West, Bethlehem, PA 18015; A. L. Drozd, ANDRO Computational Solutions, Beeches Technical Campus, Building 2, Suite 1, 7902 Turing Road, Rome, NY 13440-2067.

0018-9251/12/\$26.00 © 2012 IEEE

I. INTRODUCTION

Recent years have witnessed significant advances in multiple-input multiple-output (MIMO) wireless communication systems, which provide diversity gain and degree-of-freedom (or spatial multiplexing) gain [1, 2] by employing multiple transmit and receive antennas and space-time modulation and coding strategies. Similar ideas can be used in radar systems to improve radar performance in various ways. In general, a MIMO radar can be defined as a radar system with multiple transmit waveforms that is able to jointly process signals received at multiple receive antennas. Elements of MIMO radar transmit independent waveforms resulting in an omnidirectional beam pattern or create diverse beam patterns by controlling correlations among transmitted waveforms [3]. A MIMO radar may be configured with its antennas colocated [4] or widely distributed over an area [5]. It is shown in [6] that a radar network has the potential to achieve an improvement in signal-to-noise ratio (SNR) through coherent network sensing, and an improvement in target discrimination due to the varying target aspect. Wideband distributed coherent aperture tests and demonstrations for next generation ballistic missile defense radar have been successfully carried out [7]. In cohere-on-receive mode, an N^2 SNR gain is achieved over a single aperture; in cohere-on-transmit mode, an N^3 SNR gain is achieved [7]. In [8] it is observed that MIMO radar has more degrees of freedom than systems with a single transmit antenna. These additional degrees of freedom support flexible time-energy management modes [9], lead to improved angular resolution [10, 11], and improve parameter identifiability [12]. With widely-separated antennas, MIMO radar has the ability to improve radar detection performance by exploiting radar cross section (RCS) diversity [13], detect and estimate slow moving targets by exploiting Doppler estimates from multiple directions [14, 15], and support accurate target location and velocity estimation [16–19]. Some of the recent advances in MIMO radar have been documented in [20].

One important problem for MIMO radar systems is to localize and track targets in a certain surveillance region. In [16] the potential of MIMO radar systems to locate a single point scatterer is explored. It has been shown that a coherent MIMO radar system with widely spaced MIMO transmit and receive elements can provide a very high performance in localizing the scatterer, with an accuracy largely determined by the wavelength of the signal instead of the signal bandwidth, which determines the range estimation accuracy in a noncoherent radar system [21]. The coherent MIMO radar requires coherent signal receptions at a particular receive element, even for signals that are not transmitted by this receiving

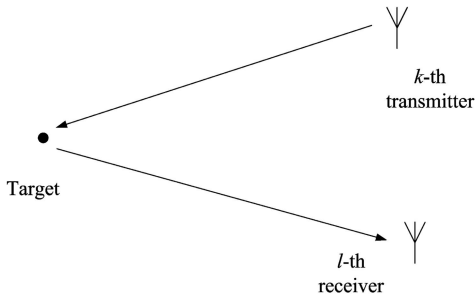


Fig. 1. Signal propagation path in MIMO radar system.

element. Since the transmitter/receiver elements are widely distributed, at a particular receiver it is difficult to maintain coherent signal waveforms of all the transmitters. Further, the reflected signal from a fading target may have an unknown phase shift, which in many cases is difficult to estimate. Considering all of these practical issues, noncoherent signal reception, which does not require the signal phase information at the receivers, is an attractive alternative. In this paper we focus on localization and tracking of a target using noncoherent MIMO radar. As demonstrated later, the noncoherent MIMO radar with widely spaced transmit and receive elements can provide localization and tracking accuracies that are significantly higher than that of a monostatic phased array radar with high range and azimuth resolutions. Further, a hybrid MIMO radar is presented, which achieves high Doppler resolution by coherently integrating only pulse trains transmitted and received by the colocated transceivers. In the hybrid MIMO radar, the pulse trains transmitted and received by non colocated transmitter-receiver pairs are combined noncoherently. In the proposed noncoherent MIMO radar system, the signals received at distributed receivers are processed jointly and the matched filter outputs are directly used for target tracking in a track-before-detect (TBD) framework. To the best of our knowledge, our work represents the first publication on TBD in MIMO radar.

The paper is organized as follows. In Section II the system model for a noncoherent MIMO radar is introduced. In Section III a maximum likelihood (ML) location and velocity estimation procedure is provided and its corresponding Cramér-Rao lower bound (CRLB) matrix is derived. Also in Section III simple Gaussian pulse waveforms with short duration are used for the MIMO radar to obtain very high localization performance, even when the corresponding matched filter ignores Doppler effect and matches to zero Doppler shift, implying significantly reduced matched filter complexity. Interactive signal processing and target tracking in a noncoherent MIMO radar system are discussed in Section IV. There, we show that for a system with high SNR and a relatively large number of transmit/receive elements, the Kalman filter (KF) delivers an optimal or near-optimal tracking

performance; for a system with a small number of elements and a low-SNR value, the particle filter (PF) is a good choice, which does not require a linear and Gaussian parametric model for the location estimates. The interaction between the tracker and the matched filters and the location estimator has been investigated. It is shown that the feedback from the tracker to the matched filter and the location estimator could significantly reduce the cost and resources required by the latter operations. The noncoherent and hybrid MIMO systems are compared with a phased array radar in terms of the tracking performance. Finally, the work is summarized in Section V.

II. SYSTEM MODEL

In this paper we investigate the localization and tracking potential of noncoherent MIMO radar with widely spaced transmit and receive elements. For simplicity, we consider a single target in a two-dimensional space, with coordinates (x, y) and velocity (v_x, v_y) . The target reflects all impinging electromagnetic (EM) waves isotropically. Suppose that there are M transmit elements and N receive elements in the MIMO radar system. Denote the coordinates of the k th transmit element as (x_k, y_k) , where $k = 1, \dots, M$, and the coordinates of the l th receive element as (x_l, y_l) , where $l = 1, \dots, N$. As illustrated in Fig. 1, the time delay of the received signal at the l th receiver due to the k th transmitter may be written as

$$\tau_{kl} = \frac{d_k + d_l}{c} \quad (1)$$

where

$$d_k \triangleq \sqrt{(x - x_k)^2 + (y - y_k)^2} \quad (2)$$

$$d_l \triangleq \sqrt{(x - x_l)^2 + (y - y_l)^2}$$

and c is the speed of the light. For nonmaneuvering targets, the Doppler shift of the received signal at the l th receiver due to the k th transmitter is

$$f_{kl} = \frac{f_c}{c} \left[\frac{v_x(x_k - x) + v_y(y_k - y)}{d_k} + \frac{v_x(x_l - x) + v_y(y_l - y)}{d_l} \right] \quad (3)$$

where f_c is the carrier frequency.

Assume that the signal transmitted by the k th transmit element is

$$s_k(t) = \sqrt{2} \text{Re} \left\{ \sqrt{E_k} \tilde{s}_k(t) e^{j2\pi f_c t} \right\} \quad (4)$$

where $\text{Re}\{\cdot\}$ denotes the real part operation and $\tilde{s}_k(t)$ is the complex envelope of the pulse transmitted by the k th transmit element. Let the complex envelope be normalized such that

$$\int_{-\infty}^{\infty} |\tilde{s}_k(t)|^2 dt = 1. \quad (5)$$

As a result the energy of the transmitted signal $s_k(t)$ is E_k .

Assuming that the number of scatterers which make up the target is large and none of them dominates, the complex envelope of the reflected signal received at the l th receive element could be modeled as a time-delayed and frequency shifted version of $\tilde{s}_k(t)$ multiplied by a complex Gaussian random variable (RV) \tilde{a}_{kl} , and

$$\tilde{a}_{kl} \sim \mathcal{CN}(0, 2\sigma_{kl}^2)$$

where $2\sigma_{kl}^2$ denotes the variance of the complex Gaussian RV. Note that the variance of \tilde{a}_{kl} reflects the cumulative effects of the antenna gain and large-scale path loss, which are deterministic. \tilde{a}_{kl} , an RV, models the fluctuation of the RCS of the target. Further, we assume that the received signal is corrupted by an additive complex white Gaussian random process $n_l(t)$

$$n_l(t) = \sqrt{2}\text{Re}\{\tilde{n}_l(t)e^{j2\pi f_c t}\} \quad (6)$$

where for simplicity and clarity of presentation, we assume that $\tilde{n}_l(t)$ is white

$$\tilde{n}_l(t) \sim \mathcal{CN}(0, N_0)$$

and

$$E[\tilde{n}_l(t)\tilde{n}_l^*(u)] = N_0\delta(t-u). \quad (7)$$

We assume that \tilde{a}_{kl} s and the $\tilde{n}_l(t)$ s are mutually independent, \tilde{a}_{kl} s are independent across different paths, indexed by the (k, l) pairs, and $\tilde{n}_l(t)$ s are independent across different receive elements.

In summary the received target signal return at the l th receive element can be written as

$$r_l(t) = \sqrt{2}\text{Re}\left\{\sum_{k=1}^M \sqrt{E_k}\tilde{a}_{kl}\tilde{s}_k(t-\tau_{kl})e^{j2\pi(f_c+f_{kl})(t-\tau_{kl})} + \tilde{n}_l(t)e^{j2\pi f_c t}\right\} \quad (8)$$

where τ_{kl} is the time delay of the received signal at the l th receiver due to the k th transmitter, which has been defined in (1), and f_{kl} is the Doppler shift corresponding to the (k, l) th path, which has been defined in (3). In the baseband, we can write the complex envelope of the received signal as

$$\begin{aligned} \tilde{r}_l(t) &= \sum_{k=1}^M \sqrt{E_k}\tilde{a}_{kl}\tilde{s}_k(t-\tau_{kl})e^{j2\pi f_{kl}t} e^{-j2\pi(f_c+f_{kl})\tau_{kl}} + \tilde{n}_l(t) \\ &= \sum_{k=1}^M \sqrt{E_k}\tilde{a}_{kl}\tilde{s}_k(t-\tau_{kl})e^{j2\pi f_{kl}t} + \tilde{n}_l(t). \end{aligned} \quad (9)$$

Note that $e^{-j2\pi(f_c+f_{kl})\tau_{kl}}$ has been absorbed in \tilde{a}_{kl} , which is a circularly symmetric Gaussian RV. Transmit elements transmit orthogonal waveforms, which

approximately maintain orthogonality even for different mutual delays and different Doppler shifts, namely

$$\int_{-\infty}^{\infty} \tilde{s}_k(t)\tilde{s}_l^*(t-\tau)e^{-j2\pi f t} dt = 0 \quad \forall k \neq l, f, \text{ and } \tau. \quad (10)$$

This implies that a receive element can separate the signals transmitted from different transmit elements, by using correlation receivers (or matched filters) that are matched to different waveforms. Even though the orthogonal waveform assumption is infeasible in practical systems, we assume that the cross-correlation of any two different waveforms is negligible while obtaining closed-form mathematical results. The degradation of localization and tracking performance due to nonnegligible cross-correlation between waveforms and its mitigation could be investigated in the future. The complex envelopes of the received baseband signals can be represented in an $N \times 1$ vector form $\tilde{\mathbf{r}}(t) = [\tilde{r}_1(t), \dots, \tilde{r}_N(t)]^T$.

III. MAXIMUM LIKELIHOOD ESTIMATION OF TARGET LOCATION AND VELOCITY

A. Theoretical Derivations

Once the received signal vector $\tilde{\mathbf{r}}(t)$ is available to the MIMO system, the target location and velocity can be estimated through the maximum likelihood estimator (MLE). Let us denote $\mathbf{x} = [x \ y \ v_x \ v_y]^T$. Since $\tilde{\mathbf{r}}(t)$ is a collection of time-continuous random signal waveforms, it is desirable to reduce it to a set of RVs. A classical solution to the problems of detection and estimation of signal waveform in the presence of noise is to represent $\tilde{r}_l(t)$, a Gaussian random process, in terms of a series expansion [22]. The MLE of the target state \mathbf{x} , which consists of its location and velocity, based on the coefficients of the series expansion has been derived and provided in the following theorem.

THEOREM 1 *The MLE of \mathbf{x} based on $\tilde{\mathbf{r}}(t)$ is*

$$\arg \max_{\mathbf{x}} \sum_{k=1}^M \sum_{l=1}^N \frac{\rho_{kl}|r_{kl}(\mathbf{x})|^2}{N_0(1+\rho_{kl})} \quad (11)$$

where

$$r_{kl}(\mathbf{x}) \triangleq \int_{-\infty}^{\infty} \tilde{r}_l(t)\tilde{s}_k^*(t-\tau_{kl}(\mathbf{x}))e^{-j2\pi f_{kl}(\mathbf{x})t} dt \quad (12)$$

and

$$\rho_{kl} \triangleq 2\sigma_{kl}^2 E_k / N_0 \quad (13)$$

is the SNR for the k , l th path.

PROOF The series expansion of the $\tilde{r}_l(t)$ can be obtained using techniques presented in [22, ch. 3].

Given a complete orthonormal set $\{\phi_1(t), \phi_2(t), \dots\}$, $\tilde{r}_l(t)$ is expanded as follows

$$\tilde{r}_l(t) = \lim_{K \rightarrow \infty} \sum_{k=1}^K r_{kl} \phi_k(t) \quad (14)$$

where

$$r_{kl} \triangleq \int_{-\infty}^{\infty} \tilde{r}_l(t) \phi_k^*(t) dt \quad (15)$$

is the coefficient corresponding to the k th orthonormal basis function, and $(\cdot)^*$ denotes the complex conjugate operation. The convergence in (14) is in mean-square sense, namely

$$\lim_{K \rightarrow \infty} E \left[\left| \tilde{r}_l(t) - \sum_{k=1}^K r_{kl} \phi_k(t) \right|^2 \right] = 0. \quad (16)$$

Now, it is natural to choose the first M orthonormal basis functions as $\tilde{s}_1(t - \tau_{1l})e^{j2\pi f_{1l}t}, \dots, \tilde{s}_M(t - \tau_{Ml})e^{j2\pi f_{Ml}t}$, respectively. Therefore, using (9) for $1 \leq k \leq M$, (15) becomes

$$\begin{aligned} r_{kl} &= \int_{-\infty}^{\infty} \tilde{r}_l(t) \tilde{s}_k^*(t - \tau_{kl}(\mathbf{x})) e^{-j2\pi f_{kl}(\mathbf{x})t} dt \\ &= \int_{-\infty}^{\infty} \left[\sum_{i=1}^M \sqrt{E_i} \tilde{a}_{il} \tilde{s}_i(t - \tau_{il}) e^{j2\pi f_{il}t} + \tilde{n}_l(t) \right] \\ &\quad \times \tilde{s}_k^*(t - \tau_{kl}(\mathbf{x})) e^{-j2\pi f_{kl}(\mathbf{x})t} dt \\ &= \sqrt{E_k} \tilde{a}_{kl} + n_{kl} \end{aligned} \quad (17)$$

where

$$n_{kl} \triangleq \int_{-\infty}^{\infty} \tilde{n}_l(t) \tilde{s}_k^*(t - \tau_{kl}) e^{-j2\pi f_{kl}t} dt. \quad (18)$$

Note that the third step of (17) follows from the assumption of orthonormal waveforms made in (5) and (10). With the same orthonormal waveform assumption and the assumption that $\tilde{n}_l(t)$ is a white complex Gaussian random process with zero mean and variance N_0 , it is easy to show that

$$E[n_{kl}] = 0 \quad (19)$$

and

$$\begin{aligned} E[n_{kl} n_{jl}^*] &= \int \int E[\tilde{n}_l(t) \tilde{n}_l^*(u)] \tilde{s}_k^*(t - \tau_{kl}) e^{-j2\pi f_{kl}t} \tilde{s}_j(u - \tau_{jl}) e^{j2\pi f_{jl}u} dt du \\ &= \int \int N_0 \delta(t - u) \tilde{s}_k^*(t - \tau_{kl}) \tilde{s}_j(u - \tau_{jl}) e^{j2\pi(f_{jl}u - f_{kl}t)} dt du \\ &= \int N_0 \tilde{s}_k^*(t - \tau_{kl}) \tilde{s}_j(t - \tau_{jl}) e^{j2\pi(f_{jl} - f_{kl})t} dt \\ &= N_0 \delta(k - j) \end{aligned} \quad (20)$$

where $\delta(\cdot)$ denotes a Dirac delta function in the second line of (20), and a Kronecker delta function in the last line. As a result,

$$n_{kl} \sim \mathcal{CN}(0, N_0) \quad (21)$$

and n_{kl} and n_{jl} are independent for all $k \neq j$. This leads directly to

$$r_{kl} \sim \mathcal{CN}(0, 2E_k \sigma_{kl}^2 + N_0) \quad (22)$$

and r_{kl} and r_{jl} are independent for all $k \neq j$.

The remaining coefficient r_{kl} s for $k > M$ can be generated by using some arbitrary orthonormal set $\{\phi_{M+1}(t), \phi_{M+2}(t), \dots\}$ whose member functions are orthogonal to $\{\tilde{s}_1(t - \tau_{1l})e^{j2\pi f_{1l}t}, \dots, \tilde{s}_M(t - \tau_{Ml})e^{j2\pi f_{Ml}t}\}$, $\forall \tau_{1l}, \dots, \tau_{Ml}$, and $\forall f_{1l}, \dots, f_{Ml}$. Hence, for $k > M$,

$$\begin{aligned} r_{kl} &= \int_{-\infty}^{\infty} \tilde{r}_l(t) \phi_k^*(t) dt \\ &= \int_{-\infty}^{\infty} \left[\sum_{i=1}^M \sqrt{E_i} \tilde{a}_{il} \tilde{s}_i(t - \tau_{il}) e^{j2\pi f_{il}t} + \tilde{n}_l(t) \right] \phi_k^*(t) dt \\ &= n_{kl}. \end{aligned} \quad (23)$$

Using the orthonormal property of $\{\phi_{M+1}(t), \phi_{M+2}(t), \dots\}$ and following a similar procedure as used in (20), it is easy to show that n_{kl} ($k > M$) and n_{jl} ($1 \leq j \leq M$) are jointly Gaussian and independent and identically distributed (IID).

The approximation of the likelihood function of $\tilde{r}_{kl}(t)$ via series expansion is not very well defined [22]. The likelihood function is proportional to the likelihood ratio, up to a factor that is not a function of \mathbf{x} , assuming that H_1 represents the signal presence hypothesis as modeled in (9), and H_0 represents the noise-only hypothesis. Hence, one can maximize the likelihood ratio, whose approximation through series expansion does not have the convergence problem, instead of the likelihood function to find the MLE of \mathbf{x} .

Define $\mathbf{r}_l = [r_{1l} \ r_{2l} \ \dots]^T$. With the fact that $r_{kl} = n_{kl}$ when either H_0 is true, or H_1 is true and $k > M$, and using (21) and (22), it is straightforward to derive the

$$\begin{aligned}
 p(\mathbf{r}_l | \mathbf{x}, H_1) &\propto \frac{p(\mathbf{r}_l | \mathbf{x}, H_1)}{p(\mathbf{r}_l | H_0)} = \prod_{k=1}^M \frac{p(r_{kl} | x, H_1)}{p(r_{kl} | H_0)} \prod_{k=M+1}^{\infty} \frac{p(r_{kl} | H_1)}{p(r_{kl} | H_0)} \\
 &= \prod_{k=1}^M \frac{N_0}{2\sigma_{kl}^2 E_k + N_0} \exp \left\{ \frac{2\sigma_{kl}^2 E_k |r_{kl}|^2}{N_0(2\sigma_{kl}^2 E_k + N_0)} \right\} \prod_{k=M+1}^{\infty} \frac{p(n_{kl})}{p(n_{kl})} \\
 &= \prod_{k=1}^M \frac{1}{1 + \rho_{kl}} \exp \left\{ \frac{\rho_{kl} \left| \int_{-\infty}^{\infty} \tilde{r}_l(t) \tilde{s}_k^*(t - \tau_{kl}(\mathbf{x})) e^{-j2\pi f_{kl}(\mathbf{x})t} dt \right|^2}{N_0(1 + \rho_{kl})} \right\}. \tag{24}
 \end{aligned}$$

Employing the assumption that $\tilde{n}_l(t)$ s are independent across receive antennas (indexed by l), we can express the likelihood function of $\tilde{\mathbf{r}}(t)$ as

$$\begin{aligned}
 p(\tilde{\mathbf{r}}(t) | \mathbf{x}, H_1) &\propto \prod_{l=1}^N \prod_{k=1}^M \frac{1}{1 + \rho_{kl}} \\
 &\times \exp \left\{ \frac{\rho_{kl} \left| \int_{-\infty}^{\infty} \tilde{r}_l(t) \tilde{s}_k^*(t - \tau_{kl}(\mathbf{x})) e^{-j2\pi f_{kl}(\mathbf{x})t} dt \right|^2}{N_0(1 + \rho_{kl})} \right\}. \tag{25}
 \end{aligned}$$

Given (25), it is straightforward to express the log-likelihood function of $\tilde{\mathbf{r}}(t)$ as

$$\begin{aligned}
 \ln p(\tilde{\mathbf{r}}(t) | \mathbf{x}, H_1) &= \sum_{k=1}^M \sum_{l=1}^N \left\{ \frac{\rho_{kl} \left| \int_{-\infty}^{\infty} \tilde{r}_l(t) \tilde{s}_k^*(t - \tau_{kl}(\mathbf{x})) e^{-j2\pi f_{kl}(\mathbf{x})t} dt \right|^2}{N_0(1 + \rho_{kl})} \right\} + c \tag{26}
 \end{aligned}$$

where c is a constant which is independent of \mathbf{x} . The MLE of \mathbf{x} , or $\hat{\mathbf{x}}(\tilde{\mathbf{r}}(t))$, is therefore

$$\arg \max_{\mathbf{x}} \ln p(\tilde{\mathbf{r}}(t) | \mathbf{x}, H_1). \tag{27}$$

From (11) or equivalently (26), it is clear that the log-likelihood of $\tilde{\mathbf{r}}(t)$ is proportional to a weighted sum of the magnitude squares of correlation-receiver (matched filter) outputs, where the correlation operations are performed for all the different combinations of $\tilde{r}_l(t)$ and $\tilde{s}_k(t - \tau_{kl}(\mathbf{x})) e^{j2\pi f_{kl}(\mathbf{x})t}$. The matched filters need a hypothesized \mathbf{x} and hence $\tau_{kl}(\mathbf{x})$ and $f_{kl}(\mathbf{x})$ to generate the reference signals. The MLE is performed by searching a grid of hypothesized \mathbf{x} s. Let us denote the dimension of \mathbf{x} as n_x , and assume that along each dimension there are N_g grid points, implying a total of $(N_g)^{n_x}$ grid points. The log-likelihood in (26) can be evaluated in either a centralized or a distributed manner. In the distributed approach, for a particular \mathbf{x} , each receiver maintains a bank of M matched filters with time-delayed and frequency-shifted versions of signals transmitted by all the transmitters as their reference signals. The

received signal at each receiver is processed locally and the weighted sums of the magnitude squares of the matched filter outputs are transmitted to a central node for all the different \mathbf{x} s. Hence, each receiver needs to perform $M(N_g)^{n_x}$ integrations. The central node collects all the local weighted sums to obtain the global weighted sum, or the log-likelihood. In the centralized approach, the signal $\tilde{\mathbf{r}}(t)$ collected at the distributed receivers are transmitted to a central processing node, where each component of $\tilde{\mathbf{r}}(t)$ is processed by a bank of correlation filters (matched filters). The log-likelihood can be readily calculated by taking a weighted sum of the magnitude squares of all the matched filter outputs. The central node needs to perform $MN(N_g)^{n_x}$ integrations. Note that during the MLE, no hard decisions (detections) are made and all the information in $\tilde{\mathbf{r}}(t)$ has been preserved. The optimal weighted sum in the MLE requires the knowledge of the SNRs (ρ_{kl} s) for all the different paths, except when all these SNRs are identical.

Now let us study the performance limit of the target location and velocity estimator in terms of the CRLB. Previously, we have derived the CRLB for the target location estimate using noncoherent MIMO radar in [23]. The CRLB for the joint location and velocity estimation problem is derived and stated in the following theorem, which is similar to the CRLB derived for MIMO radar in [24], [25].

THEOREM 2 *Assuming the existence of an unbiased estimator $\hat{\mathbf{x}}(\tilde{\mathbf{r}}(t))$, the CRLB is given by*

$$E \{ [\hat{\mathbf{x}}(\tilde{\mathbf{r}}(t)) - \mathbf{x}] [\hat{\mathbf{x}}(\tilde{\mathbf{r}}(t)) - \mathbf{x}]^T \} \geq \mathbf{J}^{-1} \tag{28}$$

in which \mathbf{J} is the Fisher information matrix (FIM)

$$\begin{aligned}
 \mathbf{J} &= \sum_{k=1}^M \sum_{l=1}^N \mathbf{J}_{kl} \\
 &= \sum_{k=1}^M \sum_{l=1}^N \frac{2\rho_{kl}^2}{1 + \rho_{kl}} \mathbf{C}_{kl} \tag{29}
 \end{aligned}$$

where

$$\begin{aligned} \mathbf{C}_{kl} &\triangleq \mathbf{A}_{kl} \mathbf{B}_k \mathbf{A}_{kl}^T \\ \mathbf{A}_{kl}^T &\triangleq \begin{bmatrix} \alpha_{kl} & \epsilon_{kl} & 0 & 0 \\ \eta_{kl} & \kappa_{kl} & \lambda_{kl} & \varphi_{kl} \end{bmatrix} \\ \mathbf{B}_k &\triangleq \begin{bmatrix} \beta_k^2 & \xi_k \\ \xi_k & \gamma_k^2 \end{bmatrix} \end{aligned} \quad (30)$$

which is called the effective bandwidth of the signal $\tilde{s}_k(t)$. It is quite clear from Theorem 2 that the location and velocity estimation accuracy is determined jointly by the SNR, the signal bandwidth, and the geometry of the target, and the transmit and receive elements.

$$\begin{aligned} \alpha_{kl} &\triangleq \frac{1}{c} \left(\frac{x-x_k}{d_k} + \frac{x-x_l}{d_l} \right) \\ \epsilon_{kl} &\triangleq \frac{1}{c} \left(\frac{y-y_k}{d_k} + \frac{y-y_l}{d_l} \right) \\ \eta_{kl} &\triangleq \frac{f_c}{c} \left[\frac{(y_k-y)[v_y(x_k-x) - v_x(y_k-y)]}{d_k^3} + \frac{(y_l-y)[v_y(x_l-x) - v_x(y_l-y)]}{d_l^3} \right] \\ \kappa_{kl} &\triangleq \frac{f_c}{c} \left[\frac{(x_k-x)[v_x(y_k-y) - v_y(x_k-x)]}{d_k^3} + \frac{(x_l-x)[v_x(y_l-y) - v_y(x_l-x)]}{d_l^3} \right] \\ \lambda_{kl} &\triangleq \frac{f_c}{c} \left(\frac{x_k-x}{d_k} + \frac{x_l-x}{d_l} \right) \\ \varphi_{kl} &\triangleq \frac{f_c}{c} \left(\frac{y_k-y}{d_k} + \frac{y_l-y}{d_l} \right) \end{aligned} \quad (31)$$

d_k and d_l have been defined in (2), and

$$\beta_k^2 = 4\pi^2 \left[\int f^2 |\tilde{S}_k(f)|^2 df - \left(\int f |\tilde{S}_k(f)|^2 df \right)^2 \right] \quad (32)$$

is the mean-square bandwidth of the transmitted signal $\tilde{s}_k(t)$, with $\tilde{S}_k(f)$ being its Fourier transform. Finally,

$$\gamma_k^2 \triangleq \int t^2 |\tilde{s}_k(t)|^2 dt - \left(\int t |\tilde{s}_k(t)|^2 dt \right)^2 \quad (33)$$

and

$$\xi_k = \text{Im} \left\{ \int t \tilde{s}_k(t) \frac{\partial \tilde{s}_k^*(t)}{\partial t} dt \right\}. \quad (34)$$

The inequality in (28) means that $E[(\hat{\mathbf{x}} - \mathbf{x})(\hat{\mathbf{x}} - \mathbf{x})^T] - \mathbf{J}^{-1}$ is a positive semidefinite matrix.

PROOF See Appendix I.

Note that β_k^2 approximately measures the frequency spread of the signal $\tilde{s}_k(t)$, and γ_k^2 measures the time spread of the signal [21]. For a real baseband signal $\tilde{s}_k(t)$, it is easy to show that the second term on the right hand side of (32) is zero. Also, according to Parseval's theorem, one has

$$\int |\tilde{S}_k(f)|^2 df = \int |\tilde{s}_k(t)|^2 dt = 1. \quad (35)$$

Therefore, for a real $\tilde{s}_k(t)$, we have

$$\beta_k = \left[\frac{\int f^2 |\tilde{S}_k(f)|^2 df}{\int |\tilde{S}_k(f)|^2 df} \right]^{1/2} \quad (36)$$

Based on (30), it can be shown that \mathbf{C}_{kl} , a 4×4 matrix, has the following elements

$$\begin{aligned} \mathbf{C}_{kl}(1,1) &= \alpha_{kl}^2 \beta_k^2 + 2\alpha_{kl} \eta_{kl} \xi_k + \eta_{kl}^2 \gamma_k^2 \\ \mathbf{C}_{kl}(1,2) &= \mathbf{C}_{kl}(2,1) = \epsilon_{kl} (\alpha_{kl} \beta_k^2 + \eta_{kl} \xi_k) \\ &\quad + \kappa_{kl} (\alpha_{kl} \xi_k + \eta_{kl} \gamma_k^2) \\ \mathbf{C}_{kl}(1,3) &= \mathbf{C}_{kl}(3,1) = \lambda_{kl} (\alpha_{kl} \xi_k + \eta_{kl} \gamma_k^2) \\ \mathbf{C}_{kl}(1,4) &= \mathbf{C}_{kl}(4,1) = \varphi_{kl} (\alpha_{kl} \xi_k + \eta_{kl} \gamma_k^2) \\ \mathbf{C}_{kl}(2,2) &= \epsilon_{kl}^2 \beta_k^2 + 2\epsilon_{kl} \kappa_{kl} \xi_k + \kappa_{kl}^2 \gamma_k^2 \\ \mathbf{C}_{kl}(2,3) &= \mathbf{C}_{kl}(3,2) = \lambda_{kl} (\epsilon_{kl} \xi_k + \kappa_{kl} \gamma_k^2) \\ \mathbf{C}_{kl}(2,4) &= \mathbf{C}_{kl}(4,2) = \varphi_{kl} (\epsilon_{kl} \xi_k + \kappa_{kl} \gamma_k^2) \\ \mathbf{C}_{kl}(3,3) &= \lambda_{kl}^2 \gamma_k^2 \\ \mathbf{C}_{kl}(3,4) &= \mathbf{C}_{kl}(4,3) = \lambda_{kl} \varphi_{kl} \gamma_k^2 \\ \mathbf{C}_{kl}(4,4) &= \varphi_{kl}^2 \gamma_k^2. \end{aligned} \quad (37)$$

B. Selection of Waveforms

The optimal waveform design for target location and velocity estimation is not the focus of this paper and could be investigated in our future work. Instead, in this paper we adopt simple Gaussian pulse waveforms to demonstrate the potential of the MIMO radar in target localization and tracking. More specifically we assume that the complex envelope of the k th transmitted signal is a Gaussian pulse with a

frequency shift $[k - (M + 1)/2]f_g$

$$\tilde{s}_k(t) = \left(\frac{1}{\pi T^2} \right)^{1/4} e^{-t^2/(2T^2)} \exp \left[j2\pi(k - (M + 1)/2)f_g t \right], \quad -\infty < t < \infty \quad (38)$$

where T is a parameter that determines the effective duration of the pulse.

Note that as long as f_g is large enough ($f_g > \beta + 2f_{\max}$), where $f_{\max} \triangleq \max_{k,l}(|f_{kl}|)$, the signals transmitted by different elements can maintain orthogonality, since equivalently they are modulated to different carrier frequencies with large enough gap (f_g) between adjacent carrier frequencies.

Based on (30) and (78), and using definitions in (32), (33), and (34), for the Gaussian pulse defined in (38), it can be shown that the FIM for estimating τ_{kl} and f_{kl} based on $\tilde{r}_{kl}(t)$ is

$$\mathbf{B}'_{kl} = \frac{2\rho_{kl}^2}{1 + \rho_{kl}} \begin{bmatrix} \frac{1}{2T^2} & 0 \\ 0 & \frac{T^2}{2} \end{bmatrix}. \quad (39)$$

From (39) it is obvious that T determines the accuracy of the delay and Doppler shift estimates of a particular Gaussian pulse waveform. A smaller T leads to better performance in delay (position) estimate, but poor performance in Doppler shift (velocity) estimate. The optimal waveform design problem, which involves the trade-off between delay and Doppler shift estimation performances, is beyond the scope of this paper. Since we assume later in the tracking examples that the uncertainty in target motion is small and the target moves at a near-constant velocity, the velocity estimate (based on a sequence of position estimates) provided by the tracker will become very accurate over time. Considering this, we choose a small T so that more accurate delay and hence position estimates can be obtained.

To be more concrete, we give an example of a MIMO radar system. The target's coordinates are [1 4] km and its velocity is [60 300] m/s. In a 3×3 MIMO system, we assume that each element consists of both a transmitter and a receiver, and the coordinates of these elements are [98.5 17.4] km, [70.7 70.7] km, and [17.4 98.5] km, respectively. The carrier frequency is $f_c = 1$ GHz. A small T is chosen, namely $T = 1.1254 \times 10^{-7}$ s. For simplicity, we further assume that each path has the same SNR value, meaning that $\rho_{kl} = \rho$, for all the (k,l) combinations. We define the SNR in dB as $10 \log_{10} \rho$.

Due to the small T chosen in the experiment, the Fisher information about Doppler shift, which is proportional to $\gamma_k^2 = T^2/2$, is negligible. More specifically, a velocity of 300 m/s along the line of sight corresponds to a Doppler shift of 1000 Hz. In comparison, at SNR of 20 dB, the CRLB on

the standard deviation (SD) of the Doppler shift estimation error is 8.9×10^5 Hz, which implies that the Doppler shift estimate is very coarse and contains little information. Using the parameters in this example, it can be shown that the FIM of \mathbf{x} defined in (29) and (37) is almost a block diagonal matrix, since $\xi_k = 0$ and γ_k^2 is very small. The entries in the upper left 2×2 block of the CRLB matrix, which corresponds to the position estimate covariance, are much smaller than those in the lower right 2×2 block of the CRLB matrix, which corresponds to the velocity estimate covariance.

Using Gaussian pulses as defined in (38), based on Theorem 1, the matched filter output can be derived as

$$\sum_{k=1}^M \sum_{l=1}^N \frac{\rho_{kl} |r_{kl}|^2}{N_0(1 + \rho_{kl})} \quad (40)$$

where

$$\begin{aligned} r_{kl} &\triangleq \sqrt{E_k} \tilde{a}_{kl} e^{-\Delta\tau_{kl}^2/(4T^2)} e^{-T^2\pi^2 \Delta f_{kl}^2} + n_{kl} \\ \Delta\tau_{kl} &= \tau_{kl} - \tau_{kl}(\mathbf{x}) \\ \Delta f_{kl} &= f_{kl} - f_{kl}(\mathbf{x}) \end{aligned} \quad (41)$$

are the mismatches between the true time delay and Doppler shift and those determined by the hypothesized \mathbf{x} , and n_{kl} has been defined in (18). It is clear from (41) that the matched filter's sensitivities to mismatches in time delay and Doppler shift are determined by T . Since we have chosen a very small T (1.1254×10^{-7} s), the matched filter cannot discern an accurate match in f_{kl} from a relatively coarse one. For example,

$$\frac{e^{-T^2\pi^2 1000^2}}{e^0} = 1 - 1.25 \times 10^{-7}.$$

This implies that a perfect match in Doppler ($\Delta f_{kl} = 0$) yields an almost identical r_{kl} to that when the mismatch is as large as 1000 Hz. Thus, in this paper, we can assume that the matched filter always matches its frequency to zero Doppler shift, and yet achieves almost the same output as if it were matched to the exact Doppler shift. Thus in the simulations throughout the paper, we use this assumption and the Doppler shift (and hence velocity) estimates are not necessary. Only the time delays are used to estimate the position of the target. Note that by ignoring all the Doppler shifts ($f_{kl}(\mathbf{x})$), by replacing them all with zeroes, the complexity of the matched filter is significantly reduced. Further, the corresponding MLE is significantly simplified, since only a position estimate is needed, and the grid search complexity is reduced from $(N_g)^4$ to $(N_g)^2$.

By ignoring Doppler shift, similar to the derivation of (26) and (27), the MLE of the target position

$\theta = [x \ y]^T$ based on the received signal $\tilde{\mathbf{r}}(t)$ can be derived as

$$\arg \max_{\theta} \sum_{k=1}^M \sum_{l=1}^N \frac{\rho_{kl} \left| \int_{-\infty}^{\infty} \tilde{r}_l(t) \tilde{s}_k^*(t - \tau_{kl}(\theta)) dt \right|^2}{N_0(1 + \rho_{kl})}. \quad (42)$$

The FIM for position estimates can be derived in a manner similar to that of Theorem 2,

$$\mathbf{J}_{\theta} = \sum_{k=1}^M \sum_{l=1}^N \frac{2\rho_{kl}^2 \beta_k^2}{1 + \rho_{kl}} \begin{bmatrix} \alpha_{kl}^2 & \alpha_{kl} \epsilon_{kl} \\ \alpha_{kl} \epsilon_{kl} & \epsilon_{kl}^2 \end{bmatrix}. \quad (43)$$

Using the parameters in this example, it is easy to show that \mathbf{J}_{θ}^{-1} is indistinguishable from the upper left 2×2 block of \mathbf{J}^{-1} . This is because in (37), $\xi_k = 0$, and γ_k^2 is negligible compared with β_k^2 , so that the Doppler shift contributes little to the estimation of target positions. We show later in the paper that even the solution with this very simple waveform leads to very accurate localization and tracking performance.

C. Simulation Results

1) *Estimation Performance versus SNR:* In the following, we give an example to illustrate the performance of the ML location estimator with various SNR values. The setup and parameters of the MIMO system have been described in Section IIIB.

In order to find the global maximum during the ML estimation formulated in (42), a systematic grid search is first employed to find an approximate global maximum point, with a complexity proportional to $(N_g)^2$. Any standard optimization algorithm could then be used to refine the search for the global maximum. The root mean square errors (RMSEs) of the ML location estimator are obtained through 1000 Monte Carlo simulations and plotted in Fig. 2, in which the theoretical CRLB on the RMSE is plotted as well. It is clear that in the log-log scale, the CRLB on the RMSE is almost a linearly decreasing function of SNR, especially for high SNR values. This is due to the fact that at high SNR, the FIM is scaled by a factor that is approximately linear in ρ , according to (29) or (43). It can also be observed that the MIMO system achieves a very high localization accuracy, with an RMSE in the order of meters for high SNR values. However, the RMSEs do not converge to the CRLBs, even for very high SNR values. This is because for the estimation problem formulated in the paper, the ML estimates are asymptotically efficient only in the classical sense, when the number of transmit/receive elements is very large, instead of in the high SNR sense [21].

To further check the efficiency of the ML estimate, we use the normalized estimation error squared (NEES) [26], which is defined as

$$\epsilon_{\theta} = (\theta - \hat{\theta})^T \mathbf{J}_{\theta} (\theta - \hat{\theta}) \quad (44)$$

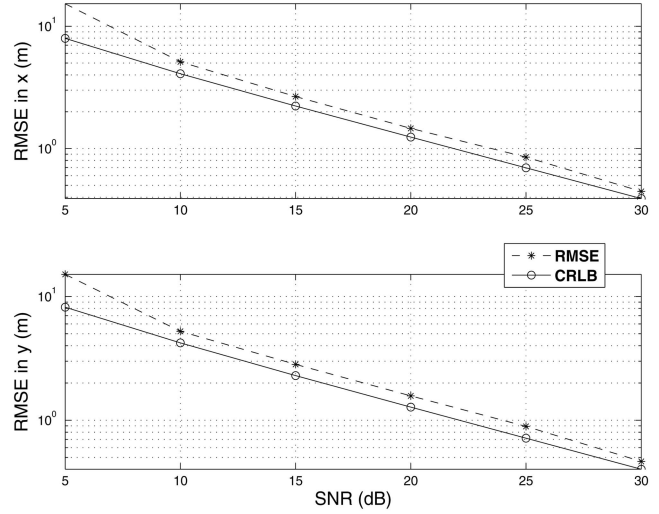


Fig. 2. RMSEs for ML estimator using a 3×3 MIMO system.

TABLE I
Average NEES Based on 1000 Monte Carlo Runs for the MLE

SNR (dB)	5	10	15	20	25	30
NEES	6.67	2.94	2.84	2.76	2.80	2.69

where $\hat{\theta}$ is the estimate, and \mathbf{J}_{θ} is the FIM. It is well known that the ML estimate is asymptotically Gaussian with the mean equal to the true value of the parameter to be estimated and variance given by the CRLB. Assuming that the estimation error is approximately Gaussian, the NEES is chi-square distributed with n_{θ} degrees of freedom, where $n_{\theta} = 2$ is the dimension of the parameter being estimated, namely θ . For multiple Monte Carlo simulations, the average of NEES is usually used, which is defined as

$$\bar{\epsilon}_{\theta} = \frac{1}{N_m} \sum_{i=1}^{N_m} \epsilon_{\theta}^i \quad (45)$$

where N_m is the number of Monte Carlo simulations. $N_m \bar{\epsilon}_{\theta}$ has a chi-square density with $N_m n_{\theta}$ degrees of freedom. Based on 1000 Monte Carlo runs, our results are listed in Table I. The two-sided 99% confidence region for the average NEES is [1.84, 2.17]. The results show that the average NEES always falls outside the two-sided 99% confidence region, even with an SNR of 30 dB. This implies that the MLE is not asymptotically efficient in the high SNR sense.

2) *Estimation Performance versus Number of Transmit/Receive Elements:* Now let us study the performance of the ML location estimator with various numbers of transmit/receive elements. In this subsection, we use the same system parameters and setup as in Section IIIC1, except that the SNR is fixed at 10 dB, and M transmit/receive elements are evenly deployed along an arc with a radius of 100 km and its origin at [0 0] km. Based on 1000 Monte

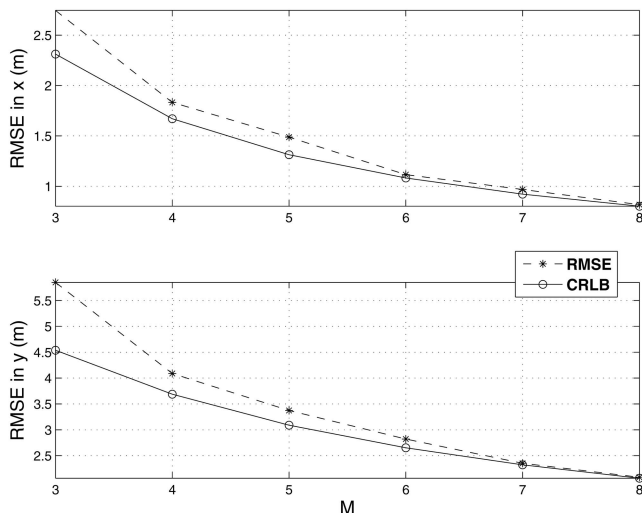


Fig. 3. RMSEs for the MLE using $M \times M$ MIMO system. SNR = 10 dB.

TABLE II
Average NEES Based on 1000 Monte Carlo Runs for the MLE

M	3	4	5	6	7	8
NEES	3.08	2.43	2.47	2.19	2.13	2.06

Carlo simulation runs, the RMSEs of the ML location estimator are obtained and plotted in Fig. 3. The theoretical CRLB on the RMSE is plotted in Fig. 3 as well. It is clear that the MIMO system achieves a very high localization accuracy, especially for a MIMO system with a large M . It can also be observed, as M increases, the RMSEs quickly approach their theoretical bounds, the CRLBs.

Based on 1000 Monte Carlo runs, the NEES for the ML location estimates are provided in Table II. The results show that for an $M \times M$ MIMO system, when M is greater than or equal to 7, the average NEES falls in the two-sided 99% confidence region. This means that the MLE is asymptotically efficient in the classical sense. That is, the errors “match” the covariance given by the CRLB for a MIMO system with a large number of transmit/receive elements.

IV. INTERACTIVE SIGNAL PROCESSING AND TARGET TRACKING

In the last section we showed that a MIMO radar system can render highly accurate target location estimates. As a sequence of such location estimates are available, it is natural to use them to infer the time-varying target state, which typically consists of target location and velocity. This process is also called target tracking and there exist many filtering techniques to solve this problem, including the KF for a linear-Gaussian tracking problem, the extended KF (EKF) [26] and unscented KF (UKF) [27] for nonlinear tracking problems, and the PF [28, 29] for the general nonlinear non-Gaussian filtering

problem. In this section, we show that for a MIMO radar system with a high SNR and a relatively large number of transmit/receive elements, the KF is very well suited to track a target with linear dynamic model, while the PF, a Monte Carlo simulation based nonparametric algorithm, is very appropriate for a MIMO radar system with a small number of transmit/receive elements and a low SNR. Note that in the proposed tracking approach, no hard decisions are made at the matched filter output. Instead, the matched filter outputs are directly used for target tracking. Hence, the proposed tracking algorithm is a TBD approach.

A. Target Dynamic Model

For simplicity and illustration purposes, in the tracking examples, we adopt a discrete-time linear and Gaussian dynamic target model. We consider a single target moving in a two-dimensional Cartesian coordinate plane. Target dynamics is defined by the 4-dimensional state vector

$$\begin{aligned} \mathbf{x}_m &= [x(t) \quad y(t) \quad \dot{x}(t) \quad \dot{y}(t)]^T|_{t=m\Delta} \\ &= [x_m \quad y_m \quad \dot{x}_m \quad \dot{y}_m]^T \end{aligned} \quad (46)$$

where m is the discrete time index, and Δ is the system sampling interval. x_m and y_m denote the coordinates of the target in the horizontal and the vertical directions with the corresponding velocities \dot{x}_m and \dot{y}_m , respectively, at time $t = m\Delta$. The superscript T denotes the transpose operation. Target motion is defined by the following widely used white noise acceleration model [26]

$$\mathbf{x}_m = \mathbf{F}\mathbf{x}_{m-1} + \mathbf{v}_{m-1} \quad (47)$$

where

$$\mathbf{F} = \begin{bmatrix} 1 & 0 & \Delta & 0 \\ 0 & 1 & 0 & \Delta \\ 0 & 0 & 1 & 0 \\ 0 & 0 & 0 & 1 \end{bmatrix} \quad (48)$$

is the state transition matrix, and \mathbf{v}_{m-1} is the process noise vector which is assumed to be white, zero-mean, and Gaussian with the following covariance matrix

$$\mathbf{Q} = q \begin{bmatrix} \frac{\Delta^3}{3} & 0 & \frac{\Delta^2}{2} & 0 \\ 0 & \frac{\Delta^3}{3} & 0 & \frac{\Delta^2}{2} \\ \frac{\Delta^2}{2} & 0 & \Delta & 0 \\ 0 & \frac{\Delta^2}{2} & 0 & \Delta \end{bmatrix} \quad (49)$$

where q denotes the power spectral density of the process noise, and indicates the process noise intensity. Note that (47) is a linear dynamic model. However, the measurement model, which is

characterized by the likelihood function provided in (25) with f_{kl} being set to zero, may or may not be deemed as linear and Gaussian, depending on whether the ML location estimation error can be deemed as additive/Gaussian or not, as explored in Sections IIIC1 and IIIC2.

B. Interactive Signal Processing and Target Tracking with a Kalman Filter

For target tracking, a sequence of measurements needs to be made over time. Here we assume that every Δ seconds, the transmit elements transmit orthogonal signals with Gaussian pulse complex envelopes that have been defined in (38). The signal returns received at all the receive elements are then processed jointly to obtain an ML estimate of the target location, as discussed in Section III. Also in Section III we have shown that for a MIMO system with a large number of transmit/receive elements, the ML location estimate can be approximately deemed as a Gaussian RV, with mean being the true target location, and covariance provided by the CRLB matrix. In this case, both target dynamic and measurement models are linear and Gaussian, rendering the KF a suitable filtering algorithm to deal with this scenario. More specifically, the tracking algorithm at each recursion includes two steps: first the target location is estimated using the MLE introduced in Section III. The ML estimate is then fed into the KF as a measurement to update the target state estimate. As a result, the measurement model is provided as

$$\mathbf{y}_m = \mathbf{H}\mathbf{x}_m + \mathbf{w}_m \quad (50)$$

where $\mathbf{y}_m \triangleq \hat{\boldsymbol{\theta}}_m = [\hat{x}_m \ \hat{y}_m]^T$ is the ML estimate of the target location,

$$\mathbf{H} = \begin{bmatrix} 1 & 0 & 0 & 0 \\ 0 & 1 & 0 & 0 \end{bmatrix} \quad (51)$$

and \mathbf{w}_m is a white Gaussian noise with covariance matrix

$$\mathbf{R}(x_m, y_m) = \mathbf{J}_{\boldsymbol{\theta}}^{-1}(x_m, y_m) \quad (52)$$

where $\mathbf{J}_{\boldsymbol{\theta}}(x_m, y_m)$ is the FIM of the ML location estimator, which is a function of the true target location $[x_m \ y_m]^T$. One problem encountered in evaluating $\mathbf{R}(x_m, y_m)$ is that $[x_m \ y_m]^T$ is the part of the unknown target state that itself needs to be estimated by the tracking filter. There are several possible solutions to this problem. One can use the estimated value of $[x_m \ y_m]^T$ to replace its true value in (52). The estimated value can be provided by the MLE of the target location as discussed in Section III, or the KF state prediction $\hat{\mathbf{x}}_{m|m-1}$ made based on measurements from time 0 to time $m-1$. Further, one can first estimate $\mathbf{R}(x_m, y_m)$ employing either one of the above methods, and then obtain the updated KF estimate

$\hat{\mathbf{x}}_{m|m}$, which in turn leads to a more accurate estimate of \mathbf{R} (namely, $\mathbf{R}(\hat{x}_{m|m}, \hat{y}_{m|m})$), which is then plugged into the KF again to obtain the final estimate $\hat{\mathbf{x}}_{m|m}$. Note the third method incurs extra complexity than the first two methods. More specifically, it requires two KF iterations at each step, the first one for a better estimate of $\mathbf{R}(x_m, y_m)$, and the second one for the final target state estimate. In the tracking example provided below, simulation results show that there are little differences in tracking performances when using different \mathbf{R} s estimated by different methods.

Next, we explore the interaction between target location estimation and target tracking. As discussed earlier the output of the ML location estimator serves as the measurement input for the tracker, based on which tracker can update its target state estimate. On the other hand, the KF at the $m-1$ th iteration can provide the state prediction $\hat{\mathbf{x}}_{m|m-1}$ and the uncertainty associated with this prediction, in the form of the covariance matrix

$$\mathbf{P}_{m|m-1} = E\{(\hat{\mathbf{x}}_{m|m-1} - \mathbf{x}_m)(\hat{\mathbf{x}}_{m|m-1} - \mathbf{x}_m)^T\}. \quad (53)$$

In other words, at time $m-1$, the KF provides prior information regarding the target position at time m . This prior information can be utilized to reduce the search space for the ML location estimator, the complexity of the optimization algorithm for MLE, and the number of matched filters required for the MLE. Here we limit the search space of the MLE by a rectangle that circumscribes an ellipse, which represents the confidence region of the predicted position with a level of confidence very close to but not equal to 100%. Mathematically, the uncertainty ellipse is represented by the following formula:

$$(\boldsymbol{\theta}_m - \hat{\boldsymbol{\theta}}_{m|m-1})^T \boldsymbol{\Sigma}_{m|m-1}^{-1} (\boldsymbol{\theta}_m - \hat{\boldsymbol{\theta}}_{m|m-1}) \leq \gamma \quad (54)$$

where $\boldsymbol{\Sigma}_{m|m-1}$ is the submatrix of the covariance matrix $\mathbf{P}_{m|m-1}$ that corresponds to the prediction of $\boldsymbol{\theta}_m$

$$\boldsymbol{\Sigma}_{m|m-1} = \begin{bmatrix} \mathbf{P}_{m|m-1}(1,1) & \mathbf{P}_{m|m-1}(1,2) \\ \mathbf{P}_{m|m-1}(2,1) & \mathbf{P}_{m|m-1}(2,2) \end{bmatrix} \quad (55)$$

and γ controls the volume of the ellipse. Since

$$\hat{\boldsymbol{\theta}}_{m|m-1} \sim \mathcal{N}(\boldsymbol{\theta}_m, \boldsymbol{\Sigma}_{m|m-1})$$

$(\hat{\boldsymbol{\theta}}_{m|m-1} - \boldsymbol{\theta}_m)^T \boldsymbol{\Sigma}_{m|m-1}^{-1} (\hat{\boldsymbol{\theta}}_{m|m-1} - \boldsymbol{\theta}_m)$ follows a χ_2^2 distribution with 2 degrees of freedom. Therefore, by setting $\gamma = F_{\chi_2^2}^{-1}(1 - \alpha)$, in which $F_{\chi_2^2}^{-1}(\cdot)$ denotes the inverse function of the cumulative distribution function (cdf) of a χ_2^2 distribution, (54) gives the $1 - \alpha$ confidence region of $\boldsymbol{\theta}_m$. For example, $\gamma = 9.21$ leads to a 99% confidence region. The rectangle which circumscribes the uncertainty region, represented

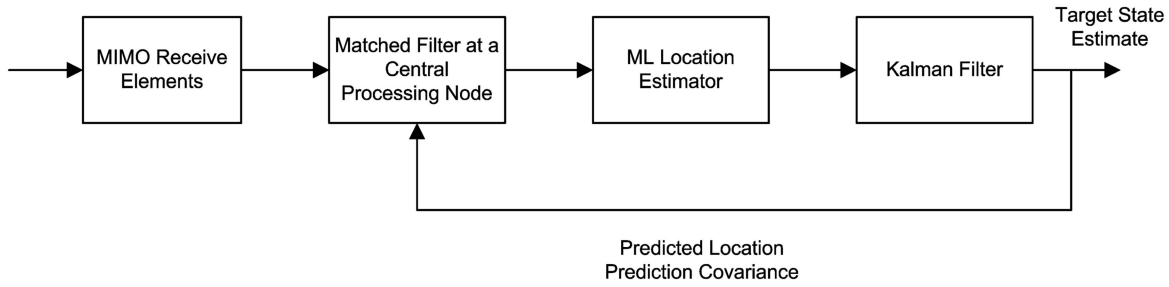


Fig. 4. Interactive signal processing and KF-based target tracking for MIMO radar systems.

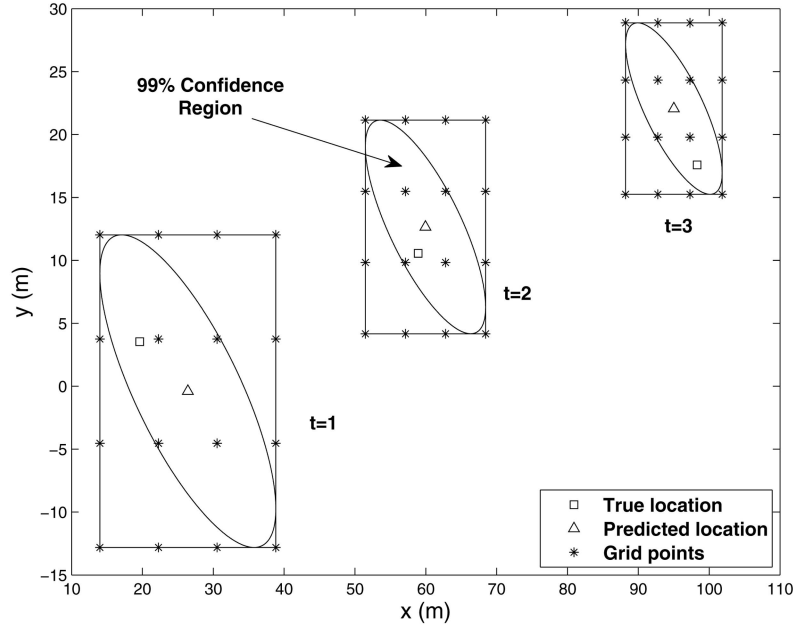


Fig. 5. Illustration of 99% confidence regions provided by KF prediction and uniform matched filter matching points.

by an ellipse as in (54), can be easily derived and provided in the following proposition.

PROPOSITION 1 *The rectangle which circumscribes the ellipse determined by (54) is*

$$\hat{x}_{m|m-1} - \sqrt{\frac{b_{22}\gamma}{b_{11}b_{22} - b_{12}^2}} \leq x \leq \hat{x}_{m|m-1} + \sqrt{\frac{b_{22}\gamma}{b_{11}b_{22} - b_{12}^2}} \quad (56)$$

and

$$\hat{y}_{m|m-1} - \sqrt{\frac{b_{11}\gamma}{b_{11}b_{22} - b_{12}^2}} \leq y \leq \hat{y}_{m|m-1} + \sqrt{\frac{b_{11}\gamma}{b_{11}b_{22} - b_{12}^2}} \quad (57)$$

where b_{11}, \dots, b_{22} denote the elements of $\Sigma_{m|m-1}^{-1}$, namely

$$\Sigma_{m|m-1}^{-1} = \begin{bmatrix} b_{11} & b_{12} \\ b_{12} & b_{22} \end{bmatrix}. \quad (58)$$

PROOF See Appendix II.

Since the target will be located in the rectangle region with a probability close to unity, the matched filter does not have to match to a position outside this rectangle. Hence, the search space of the MLE,

and the number of positions to which the matched filter at the MIMO receiver needs to match, have been significantly reduced. In summary, the interactive signal processing and target tracking MIMO radar system is illustrated in Fig. 4. The signal processing front end provides target location information, which is fed into the tracker as an input measurement. The tracker provides tracking information regarding the position and velocity of the target and feeds back the predicted prior information to the signal processing part, helping to reduce the complexity of the matched filter.

For simplicity, the rectangle area that circumscribes the confidence region of the location prediction is discretized uniformly into points in a 2-dimensional space. The ML location estimator evaluates likelihood at these points, by matching matched filter to the target locations represented by these points. In this manner, an approximate global maximum point is found, starting from which a standard optimization algorithm is then used to refine the search for the global maximum point. The 99% confidence regions provided by the KF prediction have been illustrated in Fig. 5 for three consecutive KF iterations. As we can

see, the true target location has always been located in the 99% confidence region of the KF prediction.

C. Interactive Signal Processing and Target Tracking with a Particle Filter

As shown in Section IIIC2, when the number of elements is large and the SNR is relatively high, the estimation error of the MLE can be characterized by a Gaussian noise with zero-mean and covariance matrix equal to the CRLB matrix. However, at low SNR values and with a small number of elements, this approximation is not accurate any more, as illustrated in Sections IIIC1 and IIIC2. The distribution of the ML estimation error for a nonlinear problem is in general unknown, and can only be approximated through extensive simulations. The tracking approach discussed in Section IVB is not appropriate for a system with a small number of transmit/receive elements at low SNR values, since in its measurement model, there is severe mismatch between the nominal parametric linear and Gaussian assumption described by (50) and (52) and the true nonlinear and non-Gaussian estimation errors. In such scenarios, a natural choice is to use the nonparametric sequential Monte Carlo techniques, also referred to as PFs, to track the target. In the following we provide a brief introduction to the PF that we use in the paper.

Bayesian Sequential Estimation and Particle

Filtering: Bayesian sequential estimation, also known as Bayesian filtering, is the most commonly used framework for tracking applications. In Bayesian filtering, the tracking algorithm recursively calculates the belief in the state \mathbf{x}_m based on the observations \mathbf{y} from time 1 to time m . In other words we are interested in finding the posterior distribution (or the filtering distribution) $p(\mathbf{x}_m | \mathbf{y}_{1:m})$, where $\mathbf{y}_{1:m} = \{\mathbf{y}_i, i = 1, \dots, m\}$. At each time m , the minimum mean square error (MMSE) estimate of the target state $\hat{\mathbf{x}}_{m|m}$ can be obtained by taking the expectation of \mathbf{x}_m with respect to its posterior distribution. In order to recursively calculate the posterior distribution, we need to have three distributions [28], namely the initial state distribution $p(\mathbf{x}_0)$ at time 0, the state transition model $p(\mathbf{x}_m | \mathbf{x}_{m-1})$ which represents the state dynamics and the likelihood function $p(\mathbf{y}_m | \mathbf{x}_m)$ which depends on the observation model.

In particle filtering, the main idea is to find a discrete representation of the posterior distribution $p(\mathbf{x}_m | \mathbf{y}_{1:m})$ by using a set of particles with associated weights

$$p(\mathbf{x}_m | \mathbf{y}_{1:m}) \approx \sum_{j=1}^{N_p} w_m^{(j)} \delta_{\mathbf{x}_m^{(j)}}(\mathbf{x}_m - \mathbf{x}_m^{(j)}) \quad (59)$$

where N_p is the total number of particles and $w_m^{(j)}$ is the weight of particle $\mathbf{x}_m^{(j)}$ at time m . In this paper we

employ the sequential importance resampling (SIR) particle filtering algorithm [28] to solve the nonlinear non-Gaussian Bayesian dynamic estimation problem. The advantage of the SIR PF is that it is very easy to implement and computationally more efficient compared with other variants of PFs. Here we do not discuss the details of the algorithm for brevity and refer interested readers to [28], [29] for details.

In our problem the initial set of particles is drawn from a prior distribution $\pi(\mathbf{x}_0)$ which is assumed to represent $p(\mathbf{x}_0)$. The state-space distribution $p(\mathbf{x}_m | \mathbf{x}_{m-1})$ that is needed for the prediction stage is derived by using (47). Therefore, the only remaining distribution that has to be calculated for the sequential estimation problem is the observation likelihood function $p(\mathbf{y}_m | \mathbf{x}_m^{(j)})$. In this paper the observation is a collection of matched filter outputs, namely $\tilde{\mathbf{r}}$, which has been defined in Section III. The observation likelihood function $p(\tilde{\mathbf{r}}_m | \mathbf{x}_m^{(j)})$ has been derived in Section III and provided by (25) with $f_{kl}(\mathbf{x})$ being set to zero.

Being a nonparametric tracking algorithm, the PF does not need the first and second moments of the measurements, namely the mean and the covariance matrix of the measurement to work, as opposed to the KF discussed in Section IVB. All it requires is the likelihood function $p(\mathbf{y}_m | \mathbf{x}_m^{(j)})$. Furthermore, in the PF-based tracking algorithm, there is no need to go through the two-step procedure (including location estimation and target state update), which is required by the KF. In the PF, at each iteration, the location estimate is not explicitly needed. The target location information provided by the received MIMO signal is incorporated in the filtering process through the particle weighting process. These factors make the PF very convenient and simple to implement. As a result, the PF is ideal for tracking in a MIMO radar system with a small number of transmit/receive elements and with a low-SNR value, where the linear-Gaussian measurement model is not valid any more. Once the PF updates its state estimate using MIMO radar matched filter outputs, it propagates its particles for the next time step based on (47). Analogous to the case of the KF, the matched filter will only match the positions that are determined by the propagated particles, so that the complexity and cost of the matched filter are significantly reduced. The diagram for a MIMO tracking system using a PF is shown in Fig. 6, which illustrates the interaction between the signal processing part and the particle filter.

In Fig. 7, the evolution of the particles in a PF is shown over three consecutive iterations. As can be seen, the particle “cloud” covers a region where the true target is located. In the MIMO radar the matched filters will match to the locations determined by the propagated particles as we have discussed earlier.

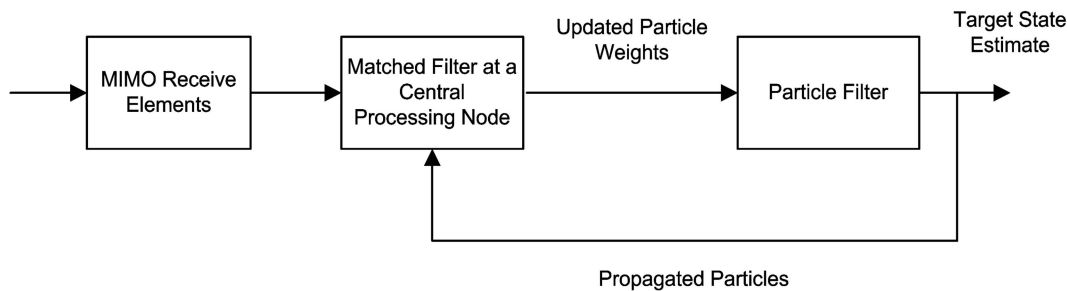


Fig. 6. Interactive signal processing and PF-based target tracking for MIMO radar systems.

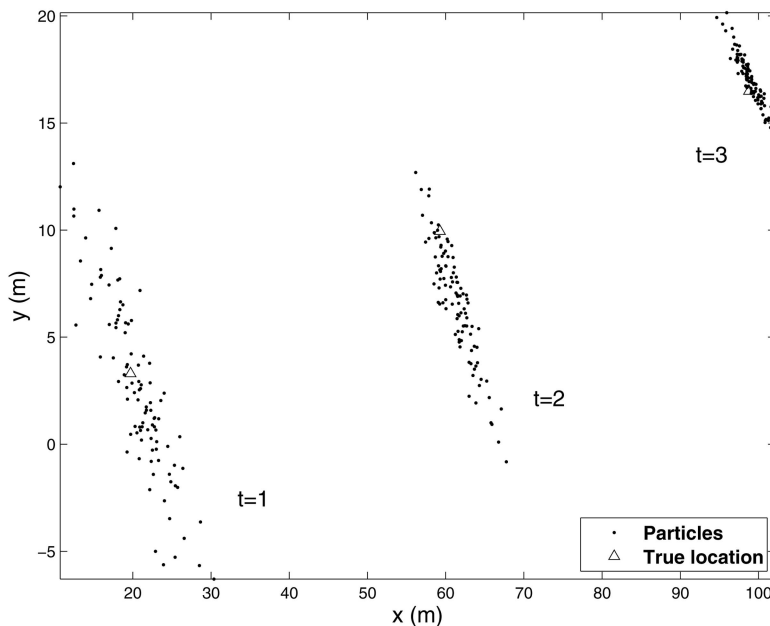


Fig. 7. Illustration of particle propagation over time.

D. Simulation Results

In this subsection, we give numerical examples for target tracking using a noncoherent MIMO radar system.

1) *5×5 MIMO Radar at High SNR*: As shown in Section IIIC2, when a MIMO system has a large number of transmit/receive elements, the measurement, namely the ML location estimate, can be deemed as linear and Gaussian, and the KF is the optimal tracking algorithm. It is known that the performance bound for any recursive nonlinear non-Gaussian tracking filter is provided by the posterior CRLB (PCRLB) [30]. The approach for recursively evaluating the PCRLB for the tracking problem formulated in this paper has been provided in Appendix IV in detail. It is also known that for a linear Gaussian problem, the KF is efficient, meaning that its RMSE can actually reach the PCRLB, which in this case coincides with the state estimate covariance matrix calculated by the KF.

Next, we give a tracking example to demonstrate the superior tracking performances provided by a noncoherent MIMO radar. We use a 5×5 noncoherent MIMO radar system, whose transmit/receive

elements are deployed as shown in Fig. 8. For the noncoherent MIMO radar system, $T = 1.1254 \times 10^{-7}$ s, and SNR = 10 dB. At time 0, the initial target position and velocity are $(-0.89, -5.02)$ km and $(59.04, 334.83)$ m/s, respectively. The target is observed for a period of 31 s, and the observations are obtained at a frequency of 1 Hz ($\Delta = 1$ s). In this case, even though the ML estimate is not efficient, as demonstrated in Section IIIC2, our results show that the KF still provides very good performance.

Both the KF discussed in Section IVB, and the PF described in Section IVC are used to track the target. For a fair comparison we set both the number of matching grid points in the KF and the number of the particles as 2000, so that the matched filters in the two cases have roughly the same complexity. Note that in the PF there is no need for the maximization step, which is, however, required in the KF case. This implies that the matched filter/KF combination results in higher complexity, since it needs to match to extra locations during the local optimization process after the grid search is performed.

In some harsh scenarios with very low SNR and a small number of elements, the tracking filters may not

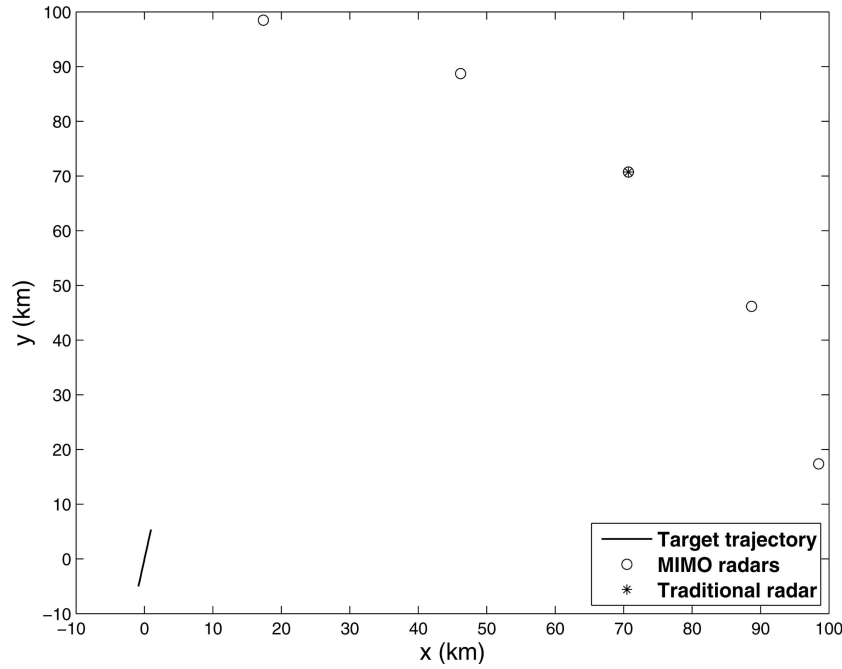


Fig. 8. Target trajectory and sensor configuration for 5×5 MIMO radar system.

keep track of the target all the time. We define that a track is lost when a filter's position estimation error (e_m) is greater than a certain threshold τ , namely

$$e_m \triangleq \sqrt{(x_m - \hat{x}_{m|m})^2 + (y_m - \hat{y}_{m|m})^2} > \tau \quad (60)$$

where $\hat{x}_{m|m}$ and $\hat{y}_{m|m}$ are the position estimates made at time m based on measurements $\mathbf{y}_{1:m}$ by the filter, and the position estimation error (e_m) keeps increasing for two consecutive time steps. Here we set $\tau = 21.21$ m.

The positional RMSE at the time step m is defined as

$$\begin{aligned} \text{RMSE}_p(m) &= \left[\frac{1}{N_f} \sum_{i=1}^{N_f} [x_m(i) - \hat{x}_{m|m}(i)]^2 + [y_m(i) - \hat{y}_{m|m}(i)]^2 \right]^{1/2}. \end{aligned} \quad (61)$$

Note that N_f is the total number of Monte Carlo runs in which the tracker maintains the track of the target from time $m = 1$ to $m = 31$, and i denotes the index for such Monte Carlo runs. The velocity RMSE is defined in a similar manner.

MIMO Radar versus High Resolution Monostatic Radar: First, the 5×5 noncoherent MIMO radar system is compared with a monostatic phased array radar with high range and bearing resolutions. We assume that in the phased array radar, a square planar array is used, which consists of L identical isotropic antennas with identical inter-antenna distance of $\lambda/2$, where λ is the wavelength corresponding to the carrier frequency. Further, for symmetry we assume that $L = (2K + 1)^2$, where K is an integer, implying that the phased array has a size of $((2K + 1)/2)\lambda \times$

$((2K + 1)/2)\lambda$. Since the transmitter and receiver in a monostatic radar are colocated, it is much easier to perform coherent pulse-Doppler processing. It is assumed that the radar transmits a coherent Gaussian pulse train to improve the Doppler resolution and to enhance the SNR through coherent integration of the pulse train. The pulse train with unit-energy and N_p Gaussian pulses is provided as follows.

$$\tilde{s}(t) = \frac{1}{\sqrt{N_p}} \sum_{i=0}^{N_p-1} \left(\frac{1}{\pi T_p^2} \right)^{1/4} e^{-(t-iT_R)^2/(2T_p^2)} \quad (62)$$

where T_p is the Gaussian pulse duration, T_R is the pulse repetition interval, which takes a value much greater than T_p ($T_R \gg T_p$). The FIM for estimating the time delay τ and Doppler shift f based on received signal $\tilde{r}(t)$ has been derived and provided in the following proposition.

PROPOSITION 2 *The FIM for estimating τ and f based on a Gaussian pulse train is*

$$\mathbf{L}_{\tau,f} = \frac{2\rho_t^2}{\rho_t + 1} \begin{bmatrix} \frac{1}{2T_p^2} & 0 \\ 0 & \frac{T_p^2}{2} + \frac{T_R^2}{12}(N_p^2 - 1) \end{bmatrix} \quad (63)$$

where ρ_t is the total SNR after coherent pulse integration.

PROOF See Appendix III.

Comparing Proposition 2 to (39), it is clear that using a pulse train instead of a single pulse, extra Fisher information $((T_R^2/12)(N_p^2 - 1))$ about the Doppler shift has been gained. Further, the azimuth (bearing) of the target can be estimated by

processing the received phased array signal. As shown in [31], for arrays of identical isotropic antennas in temporally and spatially white noise, if the square planar array's center is chosen as the origin of the Cartesian coordinate system, and the principal axes of inertia of the array are chosen as the x and y axes, then we have the FIM for estimating azimuth, time delay and Doppler shift as

$$\mathbf{L} = \begin{bmatrix} \frac{8\pi^2\rho_t}{L\lambda^2}Q & \mathbf{0} \\ \mathbf{0} & \mathbf{L}_{\tau f} \end{bmatrix} \quad (64)$$

where $\mathbf{0}$ is a zero matrix with proper dimension, $Q = Q_{xx} = Q_{yy}$ is the array configuration parameter (moment-of-inertia parameter) [31],

$$Q_{xx} \triangleq \sum_{k=1}^L (x_k - \bar{x})^2 \quad (65)$$

$$Q_{yy} \triangleq \sum_{k=1}^L (y_k - \bar{y})^2$$

$$\bar{x} = \frac{1}{L} \sum_{k=1}^L x_k = 0 \quad (66)$$

$$\bar{y} = \frac{1}{L} \sum_{k=1}^L y_k = 0$$

where (x_k, y_k) denote the coordinates of the k th antenna in the coordinate system with the origin at the center of the phased array. For the square planar array with inter-antenna distance of $\lambda/2$, it is easy to show that $Q = \lambda^2 L(L-1)/48$. Plugging Q and (63) into (64), we finally have

$$\mathbf{L} = \rho_t \begin{bmatrix} \frac{\pi^2(L-1)}{6} & 0 & 0 \\ 0 & \frac{\rho_t}{(\rho_t+1)T_p^2} & 0 \\ 0 & 0 & \frac{\rho_t}{\rho_t+1} \left[T_p^2 + \frac{T_R^2}{6}(N_p^2-1) \right] \end{bmatrix}. \quad (67)$$

Now let us determine the value of T_p for the phased array radar. For a fair comparison, it should be set as T/M , where T is the pulse duration in the

MIMO system, so that in the phased array radar, the signal bandwidth is M times that in the MIMO radar. However, in deriving (67) the narrowband assumption [31], [32] in array processing has to be satisfied, which means that the propagation time across the array is much smaller than the reciprocal of the signal bandwidth, or equivalently $\Delta\tau_{\max}/(\sqrt{2}T_p) \ll 1$, where $\Delta\tau_{\max}$ is the maximum travel time between any two elements in the array. Following this assumption and considering the specific square planar array that we assumed, it requires that $T_p \gg \sqrt{L}/(2f_c)$. Therefore, we set T_p as $T_p = \max(T/M, 5\sqrt{L}/f_c)$. To make a fair comparison, we assume that the signal power of the phased array radar is M times that of each individual transmitter used in a MIMO radar. Considering that the noise power at the receiver is $N_0 f_B$, where f_B is the signal bandwidth and is proportional to $1/T_p$, the SNR per pulse for phased array radar is MT_p/T times of the SNR for the MIMO radar system. In addition, the SNR is improved N_p -fold after the pulse train is integrated coherently. In summary, the phased array radar has a total SNR $\rho_t = (N_p MT_p/T)\rho$, where ρ is the SNR for the MIMO radar.

The monostatic radar's position is identical to that of the third transmitter/receiver element of the MIMO radar. The following parameters are used in the phased array radar: $L = 3025$, $f_c = 1$ GHz, $N_p = 25$. As a result, $T_p = 2.75 \times 10^{-7}$ s, for $\rho = 10$ dB, $\rho_t = 34.85$ dB, and the SDs in azimuth, range, and Doppler measurements are $\sigma_b = 2.57 \times 10^{-4}$ rad, $\sigma_r = 0.75$ m, and $\sigma_d = 380$ Hz, respectively.

In the case of the monostatic phased array radar, we use both an EKF and a PF to track the target. The

measurement consists of azimuth (θ), range (d_s), and Doppler shift (f_s). It can be shown that the Jacobian matrix in the EKF is

$$\mathbf{U} = (\nabla_{\mathbf{x}}[\theta \quad d_s \quad f_s])^T = \begin{bmatrix} \frac{-(y-y_s)}{d_s^2} & \frac{(x-x_s)}{d_s^2} & 0 & 0 \\ \frac{(x-x_s)}{d_s} & \frac{(y-y_s)}{d_s} & 0 & 0 \\ \frac{2f_c(y_s-y)[v_y(x_s-x) - v_x(y_s-y)]}{cd_s^3} & \frac{2f_c(x_s-x)[v_x(y_s-y) - v_y(x_s-x)]}{cd_s^3} & \frac{2f_c(x_s-x)}{cd_s} & \frac{2f_c(y_s-y)}{cd_s} \end{bmatrix} \quad (68)$$

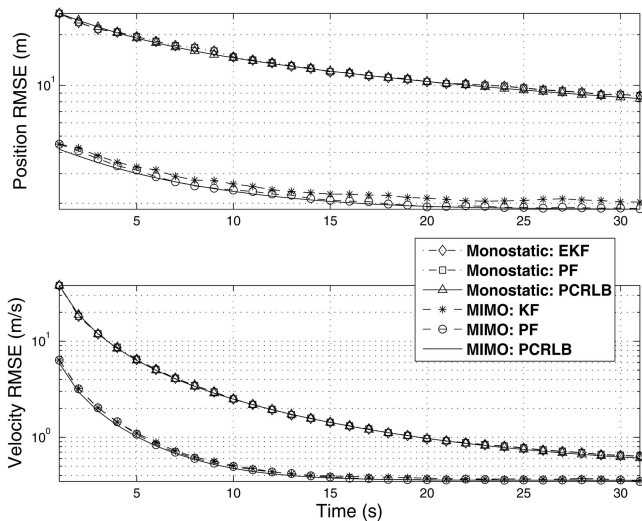


Fig. 9. RMSEs of target state estimates for 5×5 noncoherent MIMO radar system and for monostatic phased array radar. For MIMO radar: SNR = 10 dB, $T = 1.125 \times 10^{-7}$ s; for phased array radar: total SNR $\rho_t = 34.85$ dB, $N_p = 25$, $T_p = 2.75 \times 10^{-7}$ s, $T_R = 4.67 \times 10^{-6}$ s, $L = 3025$.

where (x_s, y_s) denote the coordinates of the phased array radar. For the phased array radar, the calculation of the PCRLB on the tracking estimation mean square error (MSE) has been provided in detail in Appendix IVB.

The tracking accuracies of the MIMO radar and the monostatic radar have been compared in Fig. 9. In the MIMO radar system, both the KF and the PF have an in-track percentage of 100%. Even though the PF has a slightly better tracking performance than the KF, RMSEs of both the KF and the PF are quite close to the PCRLB. This means that the KF is nearly optimal even though the estimation error of the MLE cannot be deemed as a Gaussian RV as we have shown in Section III C2. In this case, with a much smaller computational complexity, the KF is a better choice than the PF.

It is clear that the MIMO radar exhibits significant improvement in tracking accuracy. For example, at the end of the 31-s interval, the MIMO radar's RMSE for position estimate is 1.86 m, while the monostatic radar's RMSE for position estimate is 8.71 m. The inferior tracking performance of the phased array radar is mainly due to its poor cross-range accuracy. The SD of azimuth estimation error of $\sigma_b = 2.57 \times 10^{-4}$ rad corresponds to a cross-range accuracy of 25.7 m at a range of 100 km.

2) 3×3 MIMO Radar at Low SNR: Here we give tracking examples to demonstrate the superior tracking performances provided by a PF in a small MIMO radar system with low SNR. In the following tracking example, we use a 3×3 noncoherent MIMO radar system, whose transceivers coincide with the first, third, and fifth elements as shown in Fig. 8. We assume a very low SNR here, namely SNR = 5 dB.

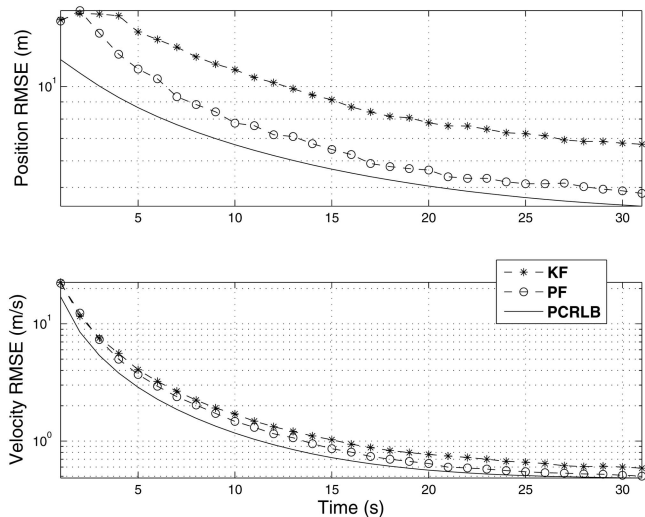


Fig. 10. RMSEs for target state estimates by 3×3 MIMO radar system. SNR = 5 dB.

TABLE III
In-Track Percentage for Various SNR Values

SNR (dB)	0	1	2	3	4	5	6
PF	41	64	86	92	96	98	99
KF	13	34	40	72	82	91	97

TABLE IV
Positional RMSE (in meters) at the end of Track for Various SNR Values

SNR (dB)	0	1	2	3	4	5	6
PF	9.29	8.96	7.02	5.79	5.77	4.80	4.01
KF	15.32	12.62	9.52	8.81	8.32	6.72	5.52

Note: RMSE is calculated only for those situations where the track is maintained until the final time step K.

In a total of 500 Monte Carlo simulation runs, the PF can keep track of the target in 490 runs while the KF in 457 runs. Further, we compare the RMSEs of these two filters, which are shown in Fig. 10. Note that these RMSEs results are obtained by taking averages over only the simulation runs where the filter keeps track of the target. It is clear that the PF has a much better tracking accuracy than the KF, especially for the positional estimates. Also plotted in Fig. 10 is the PCRLB. As expected, even the PF cannot reach the PCRLB since this is a highly nonlinear and non-Gaussian tracking problem.

Next, let us examine more tracking examples. In Table III, the in-track percentage is shown for the 3×3 MIMO system at various SNR values. Clearly, the PF can maintain a track with a much higher probability when the SNR is very low. For example, at SNR=2 dB, the PF has in-track percentage of 86%, while the KF can only achieve in-track percentage of 40%. In addition to the in-track percentage, the

RMSEs are compared for the PF and the KF. In Table IV, the positional RMSE at the final time step $m = 31$ is listed for various SNR values. Again, we can see that the PF has a much smaller RMSE. In summary, the PF outperforms the KF significantly both in terms of in-track percentage and RMSEs, especially in the severe scenario with a very low SNR and a small number of MIMO transmit/receive elements. Note that even for a small MIMO radar system operating at very low SNR, the PF can still achieve a higher tracking performance than the monostatic radar with high resolutions in range and azimuth. This is clear when Fig. 10 and Table IV are compared with Fig. 9.

E. Coherent Integration of Pulses

So far, for a MIMO system, we have assumed that a single Gaussian pulse has been used by each transmitter, and the Doppler information has been ignored. Similar to a monostatic radar a coherent pulse train can be used by the MIMO system to improve both the accuracy of the Doppler estimate and the SNR through coherent integration. In a distributed MIMO system if a signal is transmitted by a transmitter that is not colocated with the receiver, it is very difficult to coherently integrate the pulses, since the receiver needs to remember the initial phase of each pulse in the pulse train. Therefore, in this paper a hybrid MIMO system is presented, where a receiver coherently integrates the pulses transmitted by its colocated transmitter, and it processes the pulses transmitted by noncollocated transmitters noncoherently and ignores the Doppler information. As a result, in the hybrid MIMO system the FIM for estimating τ_{kl} and f_{kl} based on $\tilde{r}_{kl}(t)$ is either

$$\mathbf{B}'_{kk} = \frac{N_p^2 \rho_{kk}^2}{1 + N_p \rho_{kk}} \begin{bmatrix} \frac{1}{T_p^2} & 0 \\ 0 & T_p^2 + \frac{T_R^2}{6}(N_p^2 - 1) \end{bmatrix} \quad \forall k \quad (69)$$

or

$$\mathbf{B}'_{kl} = \frac{N_p \rho_{kl}^2}{1 + \rho_{kl}} \begin{bmatrix} \frac{1}{T_p^2} & 0 \\ 0 & 0 \end{bmatrix} \quad \forall k \neq l \quad (70)$$

where ρ_{kl} denotes the SNR per pulse for the kl th path. In the derivation of (70), we assume that each pulse in the pulse train is processed independently through noncoherent matched filter. Since the noise is assumed to be white, the matched filter outputs for different pulses in the pulse train are independent and we have an N_p -fold increase in FIM.

1) *Pulse Train with Constraint on Total SNR:* In order to separate the effect of the increased Doppler resolution by coherent pulse integration on the tracking accuracy from that of the increased SNR, we next assume that in the pulse train used either by

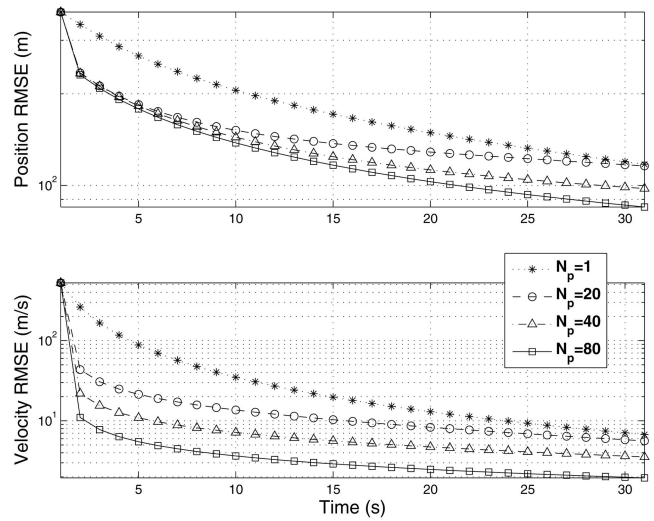


Fig. 11. PCRLBs on target state estimate RMSEs for hybrid MIMO radar. $T = 10^{-5}$ s, $T_R = 1.70 \times 10^{-4}$ s SNR = 10 dB.

the hybrid MIMO system or the phased array radar, the total SNR is a constant, which is set as 10 dB. This implies that the per pulse SNR is proportional to $1/N_p$. The PCRLBs on the target state estimate RMSEs are plotted for the hybrid MIMO system and the phased array radar in Figs. 11 and 12, respectively. It is clear that by using a pulse train, the tracking accuracy can be improved for both the MIMO system and the phased array radar, even though the total SNR is fixed. This is a result of the extra Fisher information on Doppler shift gained due to the greatly improved effective time duration of the signal as shown in (63) or (69). Comparing Fig. 11 with Fig. 12, we can see that the pulse train leads to a more pronounced improvement in MIMO radar tracking performance than that in the phased array radar. This is because that MIMO system provides more spatial diversity for signal paths with more transmitter-receiver pairs, and the improvement in Doppler resolution has an impact on all the M kk paths for $k = 1, \dots, M$.

2) Pulse Train with Constraint on Per-Pulse SNR:

Next, let us study the overall impact of the pulse train on the tracking accuracy, including both the increased Doppler accuracy and the improved SNR. For the noncoherent MIMO system, for all the kl combinations, \mathbf{B}_{kl} s are set as in (70), by ignoring the Doppler information. For both noncoherent and hybrid MIMO systems, the SNR per pulse is set as $\rho_{p1} = 3$ dB, $T_{p1} = 10^{-5}$ s, $T_{R1} = 1.70 \times 10^{-4}$ s. For the phased array radar, $T_{p2} = T_{p1}/M$, the SNR per pulse is $\rho_{p2} = MT_{p2}/T_{p1} = 1.995$ (or 3 dB), and $T_{R2} = T_{R1}$. As we can see in Fig. 13, when $N_p = 1$, all three systems provide almost the same tracking performance. As N_p increases, all three systems have more accurate tracking results. The noncoherent MIMO system has almost the same tracking performance as that of the phased array radar. The hybrid MIMO system leads to significant performance improvement in both

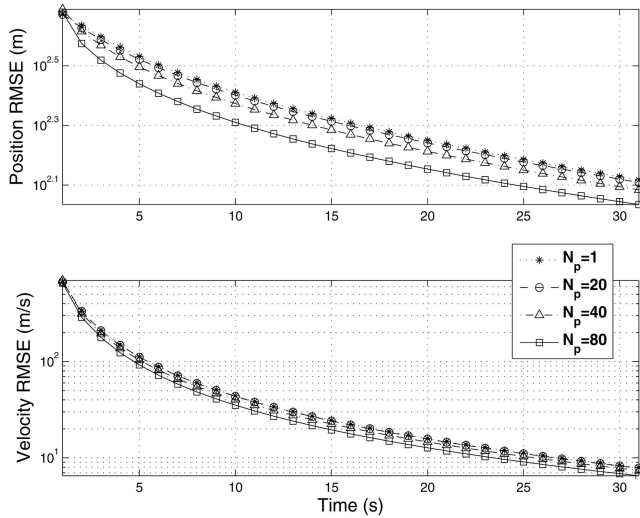


Fig. 12. PCRLBs on target state estimate RMSEs for monostatic phased array radar. $T = 2 \times 10^{-6}$ s, $T_R = 1.70 \times 10^{-4}$ s, total SNR = 10 dB.

position and velocity estimation compared with the noncoherent MIMO radar and the phased array radar. This is again due to the fact that the hybrid MIMO system gains much more Doppler shift information than the phased array radar, by integrating pulses coherently using more colocated transmitter-receiver pairs.

V. CONCLUSIONS

In this paper we have proposed localization and tracking methods for a noncoherent MIMO radar system. The MLE for the target location and velocity has been derived, and its corresponding CRLB matrix has been provided. Simple Gaussian pulse waveforms with short duration were adopted for the MIMO radar system to demonstrate MIMO radar's potential in accurate target localization. The Gaussian pulse leads to very accurate localization performance, even when the matched filter ignores the Doppler shift and matches to zero Doppler shift, which significantly simplifies its implementation. Simulation results were provided to support the theoretical derivations. Based on the localization method, we also proposed two interactive signal processing and tracking algorithms. For a system with a large number of transmit/receive elements and with a high SNR value, the KF is a good choice, since the MLE can be approximately modeled as a linear function of the target state, which is corrupted by an additive Gaussian noise. For a system with a small number of elements and a low SNR value, the PF outperforms the KF significantly, both in terms of the RMSE and in-track percentage. In both methods the tracker provides predictive information regarding the target location, so that the matched filter can match to the most probable target locations, reducing the cost and improving the tracking performance. Numerical

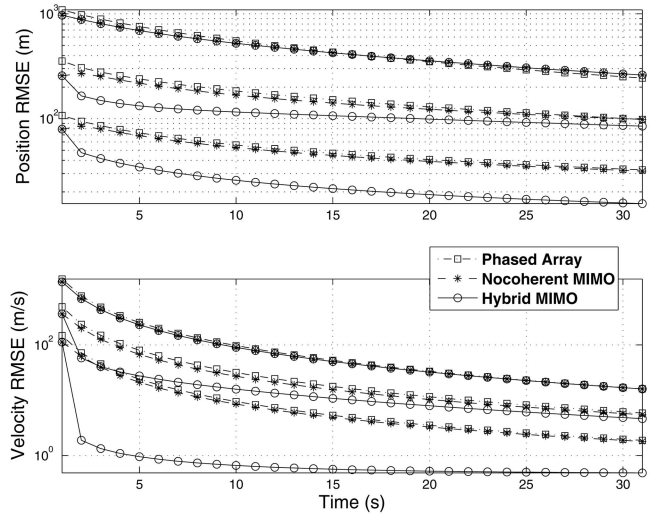


Fig. 13. PCRLBs on target state estimate RMSEs for 5×5 noncoherent MIMO radar, 5×5 hybrid MIMO radar, and monostatic phased array radar. Curves with same line type and symbols from top to bottom correspond to $N_p = 1, 10, 100$, respectively. For MIMO systems: $T_p = 10^{-5}$ s, $T_R = 1.70 \times 10^{-4}$ s, SNR_p = 3 dB; for phased array radar: $T_p = 2 \times 10^{-6}$ s, $T_R = 1.70 \times 10^{-4}$ s, SNR_p = 3 dB.

results also demonstrated that the noncoherent MIMO radar and a hybrid MIMO radar system provides significant performance improvement over a monostatic phased array radar with high range and azimuth resolutions. Future work could take into consideration the multi-target case. In addition, in this paper, the results are derived based on the white noise and orthogonal waveform assumptions. In the future, we will investigate the cases with colored noise plus clutter and waveforms with nonnegligible cross-correlations.

APPENDIX I. PROOF OF THEOREM 2

Let us first consider the Fisher information contained in signal $\tilde{r}_{kl}(t)$, namely

$$\mathbf{J}_{kl} = E[\nabla_{\mathbf{x}} \ln p(\tilde{r}_{kl}(t) | \mathbf{x}) \nabla_{\mathbf{x}}^T \ln p(\tilde{r}_{kl}(t) | \mathbf{x})]. \quad (71)$$

Using the chain rule, we have

$$\begin{aligned} \nabla_{\mathbf{x}} \ln p(\tilde{r}_{kl}(t) | \mathbf{x}) &= [\nabla_{\mathbf{x}} \tau_{kl} \quad \nabla_{\mathbf{x}} f_{kl}] \begin{bmatrix} \frac{\partial \ln p(\tilde{r}_{kl}(t) | \tau_{kl}, f_{kl})}{\partial \tau_{kl}} \\ \frac{\partial \ln p(\tilde{r}_{kl}(t) | \tau_{kl}, f_{kl})}{\partial f_{kl}} \end{bmatrix} \\ &= \mathbf{A}_{kl} \mathbf{b}_{kl} \end{aligned} \quad (72)$$

where

$$\begin{aligned} \mathbf{A}_{kl} &\triangleq [\nabla_{\mathbf{x}} \tau_{kl} \quad \nabla_{\mathbf{x}} f_{kl}] \\ \mathbf{b}_{kl} &\triangleq \begin{bmatrix} \frac{\partial \ln p(\tilde{r}_{kl}(t) | \tau_{kl}, f_{kl})}{\partial \tau_{kl}} \\ \frac{\partial \ln p(\tilde{r}_{kl}(t) | \tau_{kl}, f_{kl})}{\partial f_{kl}} \end{bmatrix} \end{aligned} \quad (73)$$

and τ_{kl} and f_{kl} are the time delay and Doppler shift of the received signal at the l th receiver due to the k th transmitter, respectively. From their definitions in (1) and (3), it is clear that τ_{kl} and f_{kl} are functions of θ . Now plugging (72) into (71), we have

$$\begin{aligned} \mathbf{C}_{kl} &= \mathbf{A}_{kl} E\{\mathbf{b}_{kl} \mathbf{b}_{kl}^T\} \mathbf{A}_{kl}^T \\ &= \mathbf{A}_{kl} \mathbf{B}'_{kl} \mathbf{A}_{kl}^T \end{aligned} \quad (74)$$

where $\mathbf{B}'_{kl} \triangleq E\{\mathbf{b}_{kl} \mathbf{b}_{kl}^T\}$.

By taking the gradient with respect to $\mathbf{x} = [x \ y \ v_x \ v_y]^T$ on both sides of (1), we get

$$\nabla_{\mathbf{x}} \tau_{kl} = \begin{bmatrix} \frac{\partial \tau_{kl}}{\partial x} \\ \frac{\partial \tau_{kl}}{\partial y} \\ \frac{\partial \tau_{kl}}{\partial v_x} \\ \frac{\partial \tau_{kl}}{\partial v_y} \end{bmatrix} = \frac{1}{c} \begin{bmatrix} \frac{x-x_k}{d_k} + \frac{x-x_l}{d_l} \\ \frac{y-y_k}{d_k} + \frac{y-y_l}{d_l} \\ 0 \\ 0 \end{bmatrix} \quad (75)$$

where d_k and d_l have been defined in (2). Similarly, by taking the gradient with respect to \mathbf{x} on both sides of (3), we have

$$\nabla_{\mathbf{x}} f_{kl} = \frac{f_c}{c} \begin{bmatrix} \frac{(y_k - y)[v_y(x_k - x) - v_x(y_k - y)]}{d_k^3} + \frac{(y_l - y)[v_y(x_l - x) - v_x(y_l - y)]}{d_l^3} \\ \frac{(x_k - x)[v_x(y_k - y) - v_y(x_k - x)]}{d_k^3} + \frac{(x_l - x)[v_x(y_l - y) - v_y(x_l - x)]}{d_l^3} \\ \frac{x_k - x}{d_k} + \frac{x_l - x}{d_l} \\ \frac{y_k - y}{d_k} + \frac{y_l - y}{d_l} \end{bmatrix}. \quad (76)$$

Combining (75) and (76) we obtain $\mathbf{A}_{kl} = [\nabla_{\mathbf{x}} \tau_{kl} \ \nabla_{\mathbf{x}} f_{kl}]$.

Note that $\mathbf{B}'_k = E\{\mathbf{b}_k \mathbf{b}_k^T\}$ is the FIM for estimating τ_{kl} and f_{kl} based on received signal $\tilde{r}_{kl}(t)$, which has been provided in [21], namely

$$\begin{aligned} \mathbf{B}'_{kl} &= \frac{2\bar{E}_r^2}{N_0(\bar{E}_r + N_0)} \begin{bmatrix} \beta_k^2 & \xi_k \\ \xi_k & \gamma_k^2 \end{bmatrix} \\ &= \frac{2\rho_{kl}^2}{1 + \rho_{kl}} \mathbf{B}_k \end{aligned} \quad (77)$$

where the identities $\bar{E}_r = 2E_k \sigma_{kl}^2$ and $\rho_{kl} = 2E_k \sigma_{kl}^2 / N_0$ have been used,

$$\beta_k^2 = 4\pi^2 \left[\int f^2 |\tilde{S}_k(f)|^2 df - \left(\int f |\tilde{S}_k(f)|^2 \right)^2 \right]. \quad (78)$$

Note that $\tilde{S}_k(f)$ is the Fourier transform of $\tilde{s}_k(t)$. Further,

$$\gamma_k^2 \triangleq \int t^2 |\tilde{s}_k(t)|^2 dt - \left(\int t |\tilde{s}_k(t)|^2 dt \right)^2 \quad (79)$$

$$\xi_k = \text{Im} \left\{ \int t \tilde{s}_k(t) \frac{\partial \tilde{s}_k^*(t)}{\partial t} dt \right\}. \quad (80)$$

Substituting (77) in (74), we finally have

$$\mathbf{J}_{kl} = \frac{2\rho_{kl}^2}{(1 + \rho_{kl})} \mathbf{A}_{kl} \mathbf{B}_k \mathbf{A}_{kl}^T = \frac{2\rho_{kl}^2}{(1 + \rho_{kl})} \mathbf{C}_{kl}. \quad (81)$$

Since \tilde{a}_{kl} and \tilde{n}_{kl} are mutually independent and they are independent across different paths, the Fisher information is additive and

$$\mathbf{J} = \sum_{k=1}^M \sum_{l=1}^N \mathbf{J}_{kl} = \sum_{k=1}^M \sum_{l=1}^N \frac{2\rho_{kl}^2}{(1 + \rho_{kl})} \mathbf{C}_{kl}. \quad (82)$$

APPENDIX II. PROOF OF PROPOSITION 1

The boundary of the uncertainty ellipse specified in (54) can be expressed as the following quadratic form

$$(\theta_m - \hat{\theta}_{m|m-1})^T \begin{bmatrix} b_{11} & b_{12} \\ b_{12} & b_{22} \end{bmatrix} (\theta_m - \hat{\theta}_{m|m-1}) = \gamma. \quad (83)$$

Now let us denote $u = x_m - \hat{x}_{m|m-1}$ and $v = y_m - \hat{y}_{m|m-1}$, we have

$$b_{22}v^2 + 2b_{12}uv + b_{11}u^2 - \gamma = 0. \quad (84)$$

Solving the above equation we get

$$v = \frac{-b_{12}u \pm \sqrt{(b_{12}^2 - b_{11}b_{22})u^2 + b_{22}\gamma}}{b_{22}}. \quad (85)$$

To obtain real solutions for the above equation, the following inequality should be satisfied

$$u^2 \leq \frac{b_{22}\gamma}{b_{11}b_{22} - b_{12}^2}. \quad (86)$$

Since $\Sigma_{m|m-1}^{-1}$ is positive definite, the inequality $b_{11}b_{22} - b_{12}^2 > 0$ holds and has been used in the derivation of (86). By symmetry, it is easy to show

that

$$v^2 \leq \frac{b_{11}\gamma}{b_{11}b_{22} - b_{12}^2}. \quad (87)$$

APPENDIX III. PROOF OF PROPOSITION 2

Provided that $T_R \gg T_p$, it could be approximately assumed that there is no overlap between adjacent Gaussian pulses since the tail of the Gaussian function decays very fast. Based on this assumption it is easy to verify that $\int |\tilde{s}(t)|^2 = 1$. Further, we have

$$\beta^2 = \int \left| \frac{\partial \tilde{s}(t)}{\partial t} \right|^2 dt - \left| \int \tilde{s}(t) \frac{\partial \tilde{s}^*(t)}{\partial t} dt \right|^2. \quad (88)$$

The first term in (88) is

$$\begin{aligned} & \int \left| \frac{\partial \tilde{s}(t)}{\partial t} \right|^2 dt \\ &= \int \frac{1}{N_p T_p^4} \left[\sum_{i=0}^{N_p-1} \left(\frac{1}{\pi T_p^2} \right)^{1/4} e^{-(t-iT_R)^2/(2T_p^2)} (t-iT_R) \right]^2 dt \\ &= \frac{1}{N_p T_p^4} \sum_{i=0}^{N_p-1} \int \left(\frac{1}{\pi T_p^2} \right)^{1/2} e^{-(t-iT_R)^2/T_p^2} (t-iT_R)^2 dt \\ &= \frac{1}{2T_p^2} \end{aligned}$$

where the second step follows the nonoverlapping Gaussian pulse assumption. Similarly, it can be shown that the second term in (88) is

$$\left| \int \tilde{s}(t) \frac{\partial \tilde{s}^*(t)}{\partial t} dt \right|^2 = 0. \quad (89)$$

Therefore, we have the (1, 1) elements of \mathbf{B} is

$$\frac{2\rho^2}{1+\rho} \beta^2 = \frac{2\rho^2}{1+\rho} \frac{1}{2T_p^2}. \quad (90)$$

The rest of the terms in \mathbf{B} can be derived in a similar manner.

APPENDIX IV. POSTERIOR CRAMÉR-RAO LOWER BOUNDS

A. PCRLB for Tracking in MIMO Radar

Let $\hat{\mathbf{x}}_m(\mathbf{y}_{1:m})$ be an estimator of the state vector \mathbf{x}_m at time m , given all the available measurements $\mathbf{y}_{1:m}$ up to time m . Then, the MSE matrix of the estimation error at time m , \mathbf{P}_m is bounded below by the PCRLB \mathbf{G}_m^{-1}

$$\mathbf{P}_m = E\{[\hat{\mathbf{x}}_m(\mathbf{y}_{1:m}) - \mathbf{x}_m][\hat{\mathbf{x}}_m(\mathbf{y}_{1:m}) - \mathbf{x}_m]^T\} \geq \mathbf{G}_m^{-1} \quad (91)$$

where \mathbf{G}_m is the FIM. In [30] Tichavský, et al. provide a recursive approach to calculate the sequential FIM \mathbf{G}_m :

$$\mathbf{G}_{m+1} = \mathbf{D}_m^{22} - \mathbf{D}_m^{21}(\mathbf{G}_m + \mathbf{D}_m^{11})^{-1}\mathbf{D}_m^{12}. \quad (92)$$

For the linear target dynamic model (47) and nonlinear measurement model explained in Section III, the recursion equations in [30] become

$$\mathbf{D}_m^{11} = E[-\Delta_{\mathbf{x}_m}^{\mathbf{x}_m} \ln p(\mathbf{x}_{m+1} | \mathbf{x}_m)] = \mathbf{F}^T \mathbf{Q}^{-1} \mathbf{F} \quad (93)$$

$$\mathbf{D}_m^{12} = E[-\Delta_{\mathbf{x}_m}^{\mathbf{x}_{m+1}} \ln p(\mathbf{x}_{m+1} | \mathbf{x}_m)] = -\mathbf{F}^T \mathbf{Q}^{-1} \quad (94)$$

$$\mathbf{D}_m^{21} = E[-\Delta_{\mathbf{x}_{m+1}}^{\mathbf{x}_m} \ln p(\mathbf{x}_{m+1} | \mathbf{x}_m)] = (\mathbf{D}_m^{12})^T \quad (95)$$

$$\begin{aligned} \mathbf{D}_m^{22} &= E[-\Delta_{\mathbf{x}_{m+1}}^{\mathbf{x}_{m+1}} \ln p(\mathbf{x}_{m+1} | \mathbf{x}_m)] \\ &\quad + E[-\Delta_{\mathbf{x}_{m+1}}^{\mathbf{y}_{m+1}} \ln p(\mathbf{y}_{m+1} | \mathbf{x}_{m+1})] \\ &= \mathbf{Q}^{-1} + \mathbf{D}_m^{22,b}. \end{aligned} \quad (96)$$

The operator Δ in (93)–(96) is defined as the second-order derivative and $\Delta_{\Psi}^{\Theta} = \nabla_{\Psi} \nabla_{\Theta}^T$. It is important to note that all the above expectations in (93)–(96) are taken with respect to the joint probability distribution $p(\mathbf{x}_{0:m+1}, \mathbf{y}_{1:m+1})$.

The initial FIM \mathbf{G}_0 can be calculated from the a priori probability density function (pdf) $p(\mathbf{x}_0)$

$$\mathbf{G}_0 = E\{-\Delta_{\mathbf{x}_0}^{\mathbf{x}_0} \ln p(\mathbf{x}_0)\}. \quad (97)$$

Based on the fact that \mathbf{x}_m , \mathbf{x}_{m+1} , and \mathbf{y}_{m+1} form a Markov chain, the joint pdf for the expectation can be rewritten as follows

$$\begin{aligned} & p(\mathbf{x}_{0:m+1}, \mathbf{y}_{1:m+1}) \\ &= p(\mathbf{x}_{0:m}, \mathbf{y}_{1:m}) p(\mathbf{x}_{m+1} | \mathbf{x}_m) p(\mathbf{y}_{m+1} | \mathbf{x}_{m+1}). \end{aligned} \quad (98)$$

Using this property along with the target dynamic and measurement models described in Sections III and IV, it is straightforward to derive $\mathbf{D}_k^{22,b}$ as

$$\begin{aligned} \mathbf{D}_k^{22,b} &= -E_{p(\mathbf{x}_m) p(\mathbf{x}_{m+1} | \mathbf{x}_m) p(\mathbf{y}_{m+1} | \mathbf{x}_{m+1})} [\Delta_{\mathbf{x}_{m+1}}^{\mathbf{x}_{m+1}} \ln p(\mathbf{y}_{m+1} | \mathbf{x}_{m+1})] \\ &= E_{p(\mathbf{x}_m) p(\mathbf{x}_{m+1} | \mathbf{x}_m)} [\Lambda(\mathbf{x}_{m+1})] \end{aligned} \quad (99)$$

where

$$\Lambda(\mathbf{x}_{m+1}) = \begin{bmatrix} \mathbf{J}_{\theta}(\mathbf{x}_{m+1}) & \mathbf{0} \\ \mathbf{0} & \mathbf{0} \end{bmatrix} \quad (100)$$

where \mathbf{J}_{θ} has been provided in (43), and $\mathbf{0}$ is a 2×2 zero matrix. The inner integrations in (99) can be approximately evaluated by converting them into summations using Monte Carlo integration methodology. In order to do this, we first generate a set of samples $\mathbf{x}_{m+1}^{(j)} \sim p(\mathbf{x}_{m+1} | \mathbf{x}_m)$ with identical weights $w_{m+1}^{(j)} = N_p^{-1}$, where $j = 1, \dots, N_p$. Then, the above expectations can be approximated as follows:

$$E_{p(\mathbf{x}_{m+1} | \mathbf{x}_m)} [\Lambda(\mathbf{x}_{m+1})] \approx \frac{1}{N_p} \sum_{j=1}^{N_p} \Lambda(\mathbf{x}_{m+1}^{(j)}). \quad (101)$$

The final expectation with respect to $p(\mathbf{x}_m)$ in (99) can be obtained by averaging the above approximations over a number of Monte Carlo trials, i.e., over a number of sample tracks.

B. PCRLB for Tracking in Phased Array Radar

For target tracking in phased array radar, the calculation of the PCRLB can be carried out in a similar manner as described in Appendix IVA, and one only needs to replace $\Lambda(\mathbf{x}_{m+1})$ in (100) with the following

$$\Lambda(\mathbf{x}_{m+1}) = \mathbf{U}^T(\mathbf{x}_{m+1})\mathbf{L}\mathbf{U}(\mathbf{x}_{m+1}) \quad (102)$$

where \mathbf{L} and \mathbf{U} have been defined in (67) and (68) respectively.

ACKNOWLEDGMENTS

The authors would like to thank Robert W. McMillan and Clifford E. Carroll for their valuable suggestions and support during the course of this work.

REFERENCES

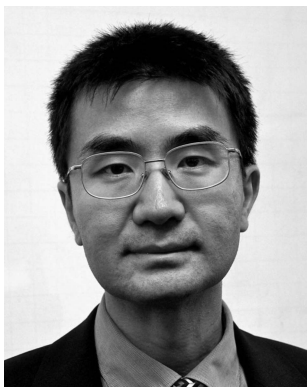
- [1] Foschini, G. J.
Layered space-time architecture for wireless communication in a fading environment when using multiple antennas.
Bell Labs Technical Journal, **1**, 2 (1996), 41–59.
- [2] Tse, D. and Viswanath, P.
Fundamentals of Wireless Communication.
New York: Cambridge University Press, 2005.
- [3] Fuhrmann, D. R. and San Antonio, G.
Transmit beamforming for MIMO radar systems using partial signal correlation.
In *Proceedings of the 38th Asilomar Conference on Signals, Systems and Computers*, Nov. 2004, 295–299.
- [4] Li, J. and Stoica, P.
MIMO radar with colocated antennas.
IEEE Signal Processing Magazine, **24**, 5 (Sept. 2007), 106–114.
- [5] Haimovich, A. M., Blum, R. S., and Cimini, L. J.
MIMO radar with widely separated antennas.
IEEE Signal Processing Magazine, **25**, 1 (2008), 116–129.
- [6] Baker, C. J. and Hume, A. L.
Netted radar sensing.
IEEE Aerospace and Electronic Systems Magazine, **18**, 2 (Feb. 2003), 3–6.
- [7] Coutts, S., et al.
Distributed coherent aperture measurements for next generation BMD radar.
In *IEEE Sensor Array and Multichannel Signal Processing Workshop*, July 2006, 390–393.
- [8] Bliss, D. W. and Forsythe, K. W.
Multiple-input multiple-output (MIMO) radar and imaging: Degrees of freedom and resolution.
In *Proceedings of the 37th Asilomar Conference on Signals, Systems and Computers*, Nov. 2003, 54–59.
- [9] Rabideau, D.
Ubiquitous MIMO digital array radar.
In *Proceedings of the 37th Asilomar Conference on Signals, Systems and Computers*, Nov. 2003, 1057–1064.
- [10] Robey, F. C., et al.
MIMO radar theory and experimental results.
In *Proceedings of the 38th Asilomar Conference on Signals, Systems and Computers*, Nov. 2004, 300–304.
- [11] Bekkerman, I. and Tabrikian, J.
Target detection and localization using MIMO radars and sonars.
IEEE Transactions on Signal Processing, **54** (Oct. 2006), 3873–3883.
- [12] Xu, L., Li, J., and Stoica, P.
Adaptive techniques for MIMO radar.
In *Fourth IEEE Workshop on Sensor Array and Multi-Channel Processing*, Waltham, MA, July 2006, 258–262.
- [13] Fishler, E., et al.
Spatial diversity in radars—Models and detection performance.
IEEE Transactions on Signal Processing, **54** (Mar. 2006), 823–838.
- [14] Lehmann, L., et al.
MIMO-radar application to moving target detection in homogenous clutter.
In *Fourth IEEE Workshop on Sensor Array and Multi-channel Processing*, Waltham, MA, July 2006.
- [15] He, Q., et al.
Cramer-Rao bound for target velocity estimation in MIMO radar with widely separated antennas.
In *Proceedings of the 42nd Annual Conference on Information Sciences and Systems*, Princeton, NJ, Mar. 2008.
- [16] Lehmann, N. H., et al.
High resolution capabilities of MIMO radar.
In *Proceedings of the 40th Asilomar Conference on Signals, Systems, and Computers*, Nov. 2006.
- [17] Godrich, H., Haimovich, A. M., and Blum, R. S.
Cramer Rao bound on target localization estimation in MIMO radar systems.
In *Proceedings of the 42nd Annual Conference on Information Sciences and Systems*, Princeton, NJ, Mar. 2008.
- [18] Godrich, H., Haimovich, A. M., and Blum, R. S.
Target localisation techniques and tools for multiple-input multiple-output radar.
IET Radar, Sonar & Navigation, **3**, 4 (2009), 314–327.
- [19] He, Q., et al.
Target velocity estimation and antenna placement for MIMO radar with widely separated antennas.
IEEE Journal of Selected Topics in Signal Processing, **4**, 1 (2010), 79–100.
- [20] Li, J. and Stoica, P. (Eds.)
MIMO Radar Signal Processing.
Hoboken, NJ: Wiley, 2008.
- [21] Van Trees, H. L.
Detection, Estimation and Modulation Theory, vol. 3.
Hoboken, NJ: Wiley, 1971.
- [22] Van Trees, H. L.
Detection, Estimation and Modulation Theory, vol. 1.
Hoboken, NJ: Wiley, 1968.
- [23] Niu, R., et al.
Target tracking in widely separated non-coherent multiple-input multiple-output radar networks.
In *Proceedings of the 43rd Annual Asilomar Conference on Signals, Systems, and Computers*, Pacific Grove, CA, Nov. 2009, 1181–1185.
- [24] He, Q., Blum, R. S., and Haimovich, A. M.
Non-coherent MIMO radar for target estimation: More antennas means better performance.
In *Proceedings of the 43rd Annual Conference on Information Sciences and Systems*, 2009, 108–113.
- [25] He, Q., Blum, R. S., and Haimovich, A. M.
Non-coherent MIMO radar for location and velocity estimation: More antennas means better performance.
IEEE Transactions on Signal Processing, **58**, 7 (July 2010), 3661–3680.
- [26] Bar-Shalom, Y., Li, X. R., and Kirubarajan, T.
Estimation with Applications to Tracking and Navigation.
Hoboken, NJ: Wiley, 2001.

- [27] Julier, S. J. and Uhlmann, J. K.
Unscented filtering and nonlinear estimation.
Proceedings of the IEEE, **92**, 3 (Mar. 2004), 401–422.
- [28] Arulampalam, M. S., et al.
A tutorial on particle filters for online
nonlinear/non-Gaussian Bayesian tracking.
IEEE Transactions on Signal Processing, **50**, 2 (Feb.
2002), 174–188.
- [29] Doucet, A., de Freitas, N., and Gordon, N. (Eds.)
Sequential Monte Carlo Methods in Practice.
New York: Springer, 2001.
- [30] Tichavsky, P., Muravchik, C. H., and Nehorai, A.
Posterior Cramér-Rao bounds for discrete-time nonlinear
filtering.
IEEE Transactions on Signal Processing, **46**, 5 (May
1998), 1386–1396.
- [31] Dogandzic, A. and Nehorai, A.
Cramér-Rao bounds for estimating range, velocity, and
direction with an active array.
IEEE Transactions on Signal Processing, **49**, 6 (June
2001), 1122–1137.
- [32] Van Trees, H. L.
*Optimum Array Processing (Detection, Estimation, and
Modulation Theory)*, Part IV.
Hoboken, NJ: Wiley-Interscience, 2002.

Ruixin Niu (M’04—SM’11) received the B.S. degree from Xi’an Jiaotong University, Xi’an, China, in 1994, the M.S. degree from the Institute of Electronics, Chinese Academy of Sciences, Beijing, China, in 1997, and the Ph.D. degree from the University of Connecticut, Storrs, in 2001, all in electrical engineering.

He is currently an assistant professor with the Department of Electrical and Computer Engineering, at Virginia Commonwealth University (VCU) in Richmond, VA. Before joining VCU, he was a research assistant professor with Syracuse University, Syracuse, NY. His research interests are in the areas of statistical signal processing and its applications, including detection, estimation, data fusion, sensor networks, communications, and image processing.

Dr. Niu received the Best Paper Award, at the Seventh International Conference on Information Fusion in 2004. He is a coauthor of the paper that won the Best Student Paper Award at the Thirteenth International Conference on Information Fusion in 2010. He is an Associate Editor of *IEEE Transactions on Signal Processing*, the Associate Administrative Editor of the *Journal of Advances in Information Fusion*, and an Associate Editor of the *International Journal of Distributed Sensor Networks*.



Rick S. Blum (S'83—M'84—SM'94—F'05) received his B.S. in electrical engineering from the Pennsylvania State University in 1984 and his M.S. and Ph.D. in electrical engineering from the University of Pennsylvania, Philadelphia, in 1987 and 1991.

From 1984 to 1991 he was a member of technical staff at General Electric Aerospace in Valley Forge, PA, and he graduated from GE's Advanced Course in Engineering. Since 1991, he has been with the Electrical and Computer Engineering Department at Lehigh University in Bethlehem, PA, where he is currently a professor and holds the Robert W. Wieseman Chaired Research Professorship in Electrical Engineering. His research interests include signal processing for communications, sensor networking, radar and sensor processing.

Dr. Blum is on the editorial board for the *Journal of Advances in Information Fusion* of the International Society of Information Fusion. He was an associate editor for *IEEE Transactions on Signal Processing* and for *IEEE Communications Letters*. He has edited special issues for *IEEE Transactions on Signal Processing*, *IEEE Journal of Selected Topics in Signal Processing* and *IEEE Journal on Selected Areas in Communications*. He is a member of the SAM Technical Committee (TC) of the IEEE Signal Processing Society. He was a member of the Signal Processing for Communications TC of the IEEE Signal Processing Society and is a member of the Communications Theory TC of the IEEE Communication Society. He was on the awards Committee of the IEEE Communication Society. He is an IEEE Third Millennium Medal winner, a member of Eta Kappa Nu and Sigma Xi, and holds several patents. He was awarded an ONR Young Investigator Award in 1997 and an NSF Research Initiation Award in 1992. His IEEE Fellow Citation "scientific contributions to detection, data fusion and signal processing with multiple sensors" acknowledges some early contributions to the field of sensor networking.



Pramod K. Varshney (F'97) was born in Allahabad, India, on July 1, 1952. He received the B.S. degree in electrical engineering and computer science (with highest honors) and the M.S. and Ph.D. degrees in electrical engineering from the University of Illinois at Urbana-Champaign in 1972, 1974, and 1976, respectively.

Since 1976, he has been with Syracuse University, Syracuse, NY, where he is currently a Distinguished Professor of Electrical Engineering and Computer Science. His current research interests are in distributed sensor networks and data fusion, detection and estimation theory, wireless communications, image processing, radar signal processing, and remote sensing.

Dr. Varshney is the author of *Distributed Detection and Data Fusion* (New York: Springer-Verlag, 1997). He was a James Scholar, a Bronze Tablet Senior, and a fellow while with the University of Illinois. He is a member of Tau Beta Pi and is the recipient of the 1981 ASEE Dow Outstanding Young Faculty Award. He was the guest editor of the special issue on Data Fusion of the *Proceedings of the IEEE*, January 1997. In 2000 he received the Third Millennium Medal from the IEEE and the Chancellor's Citation for Exceptional Academic Achievement at Syracuse University. He serves as a distinguished lecturer for the IEEE Aerospace and Electronic Systems (AES) Society. He is on the editorial boards of the *International Journal of Distributed Sensor Networks* and the *IEEE Transactions on Signal Processing*. He was the President of the International Society of Information Fusion during 2001.



Andrew L. Drozd (M'85—SM'96—F'02) received a Bachelor's Degree in physics and mathematics in 1977 and a Master's Degree in electrical engineering majoring in communications/signal processing in 1982, both from Syracuse University, Syracuse, NY.

He is the President/CEO and Chief Scientist of ANDRO Computational Solutions, LLC. His responsibilities include systems engineering, computational electromagnetics, software algorithm development, and use of AI/expert system technologies for developing next-generation cognitive communications and sensor suites focusing on dynamic shared spectrum techniques. From 1984 to 1994, he was a senior scientist at Kaman Sciences Corporation where he managed an engineering group. Prior to that he was a lead engineer for General Electric in Syracuse, NY. During 1983 to 1984 he was an instructor for Syracuse University teaching courses on electromagnetics and physical optics. From 1978 to 1983, he was the lead engineer for the IIT Research Institute Intrastandard Analysis Program Support Center which was responsible for maintaining the inventory of U.S. Air Force electromagnetic software codes. During the period 1976 to 1978, he was a technical assistant for the USAF Rome Air Development Center (RADC, now AFRL) where he was involved in performing testing and computer simulations of HF/VHF circuit parasitics. He is the Past President of the IEEE EMC Society, member of the IEEE Standards Association Standards Board, and is the current Chair of the IEEE EMC-S Standards Development Committee. He has authored over 150 technical papers, reports, and articles.

